Earth system feedback mechanisms and maximization of entropy production within a zonal energy balance model

JORDY VAN DER POL

Thesis for the Master Climate Studies with Earth System Science thesis track
Wageningen University
Supervisor: Laurens Ganzeveld
MAQ-81336

As opposed to isolated systems, the Earth is maintained in a steady-state far away from its thermodynamic equilibrium. It is hypothesized that this state reflects a state of maximum entropy production. In this study, we examined this maximum entropy production principle (MEPP) using an expanded version of Budyko's nine-box energy balance including, among others, the cloud and water vapor feedback mechanisms as well as diagnostic calculations of entropy production associated with heat transport following two separate methods. With this system, we assessed whether the MEPP is satisfied in Budyko's model, focusing on the role of the implemented feedback mechanisms and on its application to the faint young sun paradox.

We were unable to successfully reproduce the current climate while constraining the heat transport constant by the MEPP, neither were we able to successfully apply the MEPP in order to explore the faint young sun paradox in our model. However, our results did bring to light the imperative role of the ice albedo feedback in determining the moment at which the model reaches a local maximum in entropy production. We further illustrate how the behavior of entropy production as function of the heat transport constant can be characterized by our implemented feedback mechanisms. In addition, we propose the possibility that entropy production can perhaps better be seen as a direction in which a system like the Earth evolves in response to changes in forcings and Earth system dynamics rather than explaining its current state.

Keywords: Entropy production, energy balance model, ice albedo feedback, water vapor feedback, cloud feedback, heat transport
March 27, 2017

1 Introduction

When looking at the Earth, one can see erosion of mountains, heat being transported from the equator to the poles, and biological material breaking down. What these processes have in common, is that they all seem to develop in the same direction, but also show to be irreversible in nature. Each of these processes perform work to minimize gradients present on Earth. A thermodynamic equilibrium (TE) can be expressed as a state in which all gradients have vanished, and all these aforementioned processes seem to work towards this state. However, in its current state, the Earth has clearly not yet reached a TE. The atmospheric composition for example currently consists of an average

relative humidity of 60% and an oxygen content of 21%. However, in TE, all oxygen would have disappeared through means of oxidation, and the atmosphere would gain moisture until saturation is reached (Kleidon, 2012).

Thermodynamic processes produce entropy until a TE is reached, in which entropy is at its maximum. So why can the Earth constantly produce entropy and at the same time not reach TE? The second law of thermodynamics states that the entropy of an isolated system can either increase or remain constant when in a steady state. However, the earth is not an isolated system, but undergoes an ongoing exchange of energy as well as an exchange of entropy with its surrounding. This exchange of energy can be seen as the ultimate driving force behind system Earth's ability to maintain a state far away from TE (Kleidon, 2010). Lovelock (1965; 1975) has even suggested that this state far away from a TE, as found on Earth, is a sign of the presence of widespread life. He put forward the possibility to use it as a tool to recognize signs of life on extraterrestrial planets.

The exchange of entropy with its surrounding enables the Earth to keep producing entropy through thermodynamic processes but still preserve its state far away from TE. It raises the question how far away the Earth is from a TE. To answer this, the maximum entropy production principle (MEPP) has been proposed by Paltridge (1975, 1978). The MEPP states that thermodynamic processes on Earth produce entropy at their maximum rate, hinting at the notion that the Earth is as far as possible away from a state of TE (Kleidon, 2010).

To illustrate this, we show in Figure 1 the meridional heat flux as a function of TE on Earth. When the rate of meridional energy transport approaches infinity, the Earth becomes isothermal, that is, with a lack of temperature gradients (i.e. the Earth reaches a TE in relation to temperature). Consequently, due to a lack of meridional heat transport, entropy production in this isothermal state becomes zero and the total entropy has reached its maximum. At the other end of the scale you find an Earth without any heat transport, which physically speaking is an unrealistic outcome. What Figure 1 portrays is the idea that potentially a broad range in rates of meridional heat transport exists, but as can be inferred from observations, the Earth is presently in a state with strong mixing and stormy conditions. The rate at which the Earth's atmospheric dynamics operate, is a rate where maximum work is performed and thus also a rate that results in maximum entropy production. A clear explanation of the MEPP has been given by Kleidon et al. (2010): *"...if there are sufficient degrees of freedom, that is, sufficient choice among steady-states that all meet the fundamental conservation laws, the system would be characterized by a maximization of entropy production"*.

The MEPP has already been evaluated for a wide range of topics (Paltridge, 1975, 1978; Paltridge et al., 2007; Nicolis and Nicolis, 1980; Noda and Tokioka, 1983; Wyant et al., 1988; Gerard et al., 1990; O'brien and Stephens, 1995; Lorenz et al., 2001; Pujol, 2002; Kleidon, 2004, 2010; Dyke, 2008; Meysman and Bruers, 2010; Porada et al., 2011; Pascale et al., 2012)

Paltridge (1975) and Nicolis and Nicolis (1980) for example showed how the Earth's meridional energy flux can be predicted with extraordinary accuracy by application of the MEPP. Gerard et al. (1990) have used the MEPP to study the ongoing so-called *"climatic paradox of the faint young sun"*. They showed that when meridional heat transport is constrained by the MEPP, there is a possibility that the Earth was never fully covered in ice. The MEPP prevents the system from a full glaciation over an extended range of values for the solar luminosity, hereby increasing the Earth's stability, i.e. the Earth's state of a partly glaciated surface is proven to be more stable compared to models not based on the MEPP. A full glaciation can be prevented by decreasing the heat flux between the lower and higher latitudes, allowing more heat to stay in the lower latitudes and thus preventing it from a glaciation.

Another example of how application of the MEPP can provide useful insight in Earth system dynamics is a research conducted by Lorenz et al. (2001). In their study, a simple two-box model is used to represent the Earth's meridional heat flux, as well as that of Titan and Mars, in which the meridional heat flux was constrained by the MEPP. Their model simulations resulted in inferred zonal temperatures and heat flows in accordance with observed values for all three planets.

What these examples have in common, is the idea that one simple principle can be used to model complex phenomena in situations where detailed information is lacking. However, not all studies report a successful application of the MEPP. Meysman and Bruers (2010) applied the principle to living systems. Although they did show that living systems occur in a state of higher entropy production than abiotic systems, they also found that an increase in the complexity of ecosystems (i.e. more trophic levels) cannot directly be linked to an enhanced entropy production compared to an ecosystem lacking this complexity.This, however, does not necessarily negatively reflect on the MEPP. As Goody (2007) mentioned, it is essential to define the applicability of the MEPP before it can be applied with confidence. The results apprehended by Meysman and Bruers (2010) can help to further define the applicability of the MEPP.

In the ideal situation, all parameters describing the functioning of system Earth and its many processes are known and are measurable. However, for the Earth this is not the case, let alone for extraterrestrial planets. Nevertheless, one way to further enhance our understanding and ability to represent Earth system dynamics, is by use of the proposed principle of maximum entropy production. As put forward by Kleidon (2009), the MEPP can be seen as generally applicable and able to postulate simple behavior in complex systems.

As previously discussed, a wide range of studies have applied the MEPP to fairly simple energy balance models Paltridge (1975, 1978); Gerard et al. (1990); Lorenz et al. (2001); Pujol (2002); Dyke (2008). However, as Wyant et al. (1988) mentioned in his article, the applicability of the MEPP still needs to be determined within models considering climate interaction, focusing on non-linear modeled interactions in particular. Although a physical support is still lacking for the MEPP, by use of information theory, Dewar (2003, 2005) was able to show statistically that for systems away from a TE, the most probable state is one of maximum entropy production. This statistical prove substantiates the MEPP, increasing the importance of a further assessment of its applicability. Here we plan to build on previous work, by sticking with a simple energy balance model, but extending it through the explicit inclusion of three well-known critical feedback mechanisms and aim to increase our ability in assessing the applicability of the MEPP.

A modified version of the energy balance model by Budyko (1969) will be used. The following three feedback mechanisms will be implemented and analyzed: the ice-albedo feedback (already present) , the cloud feedback, and the water vapor feedback. At first we will apply the MEPP to the model without presence of feedback mechanisms, to confirm previous results by others. Afterwards, entropy production will be analyzed as function of the various feedback mechanisms. In this study we also aim to assess to what extent consideration of these feedback mecha-

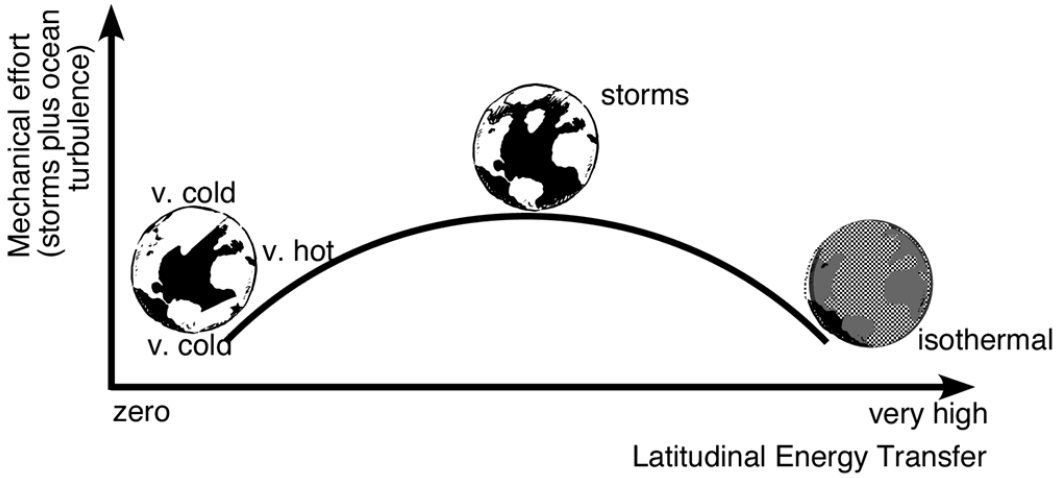

Figure 1: The mechanical effort as function of meridional heat transport. SOURCE MISSING

nisms further informs us, comparable to a study by Gerard et al. (1990), who has examined the *"climatic paradox of the faint young sun"* while solely including the ice albedo feedback. Here, the same test will be performed with either solely the ice albedo feedback mechanism, as well as combined with both of the other two feedback mechanisms.

2 The model

The model developed for this study is an altered version of the energy balance model designed by Budyko (1969). Budyko's one dimensional energy balance model aims at determining the Earth's latitudinal surface temperature distribution. Calculation of incoming shortwave radiation, outgoing longwave radiation, and heat flux for each zone in the model, enables the setup of a zonal energy balance and subsequently the calculation of the surface temperature. The same principle was applied here.

Originally, Budyko's model solely consisted of the northern hemisphere divided into nine boxes, each spanning 10°. However, the model developed here is extended towards a full global model consisting of eighteen boxes, including differences in some of the essential parameters for each hemisphere. One important assumption made here is the lack of heat transport across the poles and across the equator. For a list of the parameters and certain reference values used in the model, see Appendix A and Table 1.

2.1 *Base model*

Within Budyko's model, the equation used for zonal surface temperature calculations is:

$$T_{s,i} = \frac{Q_i(1-\alpha_{z,i}) - A + k_t T_p}{B + k_t}, \quad (1)$$

where i=1:18 represent the eighteen zones in our model, Q_i the zonal incoming solar radiation, $\alpha_{z,i}$ the zonal albedo, A and B reflect the loss of energy by black body radiation, k_t is the heat transport constant, and T_p is the planetary average surface temperature. However, to allow for the implementation of the cloud and water vapor feedback, within Equation (1) the incoming radiation ($Q_i(1-\alpha_{z,i})$) has been adapted:

$$T_{s,i} = \frac{F_{in,wv,i} - A_{n/s} + k_t T_p}{B_{n/s} + k_t}. \quad (2)$$

Here $F_{in,wv,i}$ represents the total incoming radiation which is calculated through:

$$F_{in,wv,i} = Q_i(1 - Cc_i\alpha_{c,i})(1-\alpha_{s,i}) + Wv_i, \quad (3)$$

Cc_i represents the zonal cloud cover, $\alpha_{c,i}$ the zonal cloud albedo, $\alpha_{S,i}$ the zonal surface albedo, and Wv_i the enhancement in incoming radiation due to the water vapor feedback. The rewritten calculation of temperature according to Equation (2) allows a direct implementation of both feedback mechanisms through the parameters Cc_i and $LW_{wv,i}$, representing the cloud and water vapor feedback respectively. $\alpha_{z,i}$, which originally corresponded to the total albedo of the zone in question, is now split into separate albedo values for either the zone's surface ($\alpha_{s,i}$) or clouds ($\alpha_{c,i}$). This enabled the inclusion of cloud cover (Cc_i) within the zonal temperature calculations through multiplication with cloud albedo.

In Equation (2) as well as in subsequent equations, parameters A and B were replaced with A_n and B_n for the northern hemisphere, and with A_s and B_s for the southern hemisphere (indicated as $A_{n/s}$ and $B_{n/s}$). This is needed to recreate the distinct temperature patterns observed for each hemisphere, as was done by Cess (1976). In order to simulate realistic temperatures in the model, the chosen values for the constants A_n, B_n, A_s and B_s were slightly adapted with respect to values used by Budyko. However, these new values only differ by a few percent from values used by for example Budyko (1969); Cess (1976); Chỳlek and Coakley Jr (1975); North et al. (1981, 1983); Walsh and Rackauckas (2015) in similar energy balance models.

The equation used to calculate the average planetary temperature is adapted from Budyko according to:

$$T_p = \frac{\frac{Q}{4}(1-\alpha_p) - A_{n/s}}{B_{n/s}}, \quad (4)$$

with Q representing the solar constant and α_p the planetary albedo. The planetary albedo is a fixed constant within Budyko's model, however for diagnostic purposes and to enable the calculations of snowball Earth it is made more explicit here by calculating it in each iteration through:

$$\alpha_p = \sum_{i=1}^{18} Z_i(Cc_i\alpha_{c,i} + \alpha_{s,i}(1-Cc_i)), \quad (5)$$

Table 1: Reference parameters used in the model.

Latitude [°]	T [K]	Surface area [km^2] e6	$\alpha_{s0,i}$	$Cc_{0,i}$	$\alpha c0,i$
North					
80-90	252.63	3.908	0.61	0.62	0.642
70-80	258.63	11.594	0.61*	0.66	0.627
60-70	267.24	18.905	0.24	0.65	0.534
50-60	275.51	25.706	0.14	0.60	0.509
40-50	283.11	31.497	0.12	0.53	0.464
30-40	290.41	36.405	0.10	0.46	0.459
20-30	296.00	40.198	0.10	0.43	0.419
10-20	299.16	42.778	0.09	0.47	0.383
0-10	299.63	44.084	0.08	0.52	0.354
South					
0-10	298.91	44.084	0.07	0.52	0.339
10-20	297.25	42.778	0.08	0.48	0.344
20-30	292.91	40.198	0.08	0.48	0.381
30-40	287.41	36.405	0.08	0.54	0.429
40-50	282.00	31.497	0.07	0.66	0.463
50-60	274.36	25.706	0.17	0.72	0.481
60-70	264.66	18.905	0.21	0.76	0.565
70-80	252.85	11.594	0.63	0.65	0.660
80-90	243.10	3.908	0.84	0.54	0.650

T: sea surface temperature of each zone, obtained from Haurwitz and James (1944)
α_s: surface albedo for each zone, obtained from Sellers (1965)
C_c: Cloud cover for each zone, obtained from Sellers (1965)
α_c: cloud albedo for each zone, obtained from Cess (1976)
** This values has been adjusted to represent the albedo of ice in the model as the reference temperature in this box is beneath 263K (T_{crit}).*

with Z_i representing the relative zonal contribution to the total planetary albedo.

2.2 *Feedback mechanisms*

2.2.1 Ice albedo feedback

The ice albedo feedback mechanism that already exists in Budyko's model is kept mostly unchanged. The feedback is parameterized as a step function checking whether or not the temperature of each of the eighteen zones during each iteration is below a certain threshold temperature. This is implemented as

$$\alpha_{s,i} = \begin{cases} \alpha_{ground,i} & \text{if } T_{s,i} \geq 263 \text{ K} \\ \alpha_{ice} & \text{if } T_{s,i} < 263 \text{ K}, \end{cases} \quad (6)$$

where α_{ice} represents the albedo of ice, and $\alpha_{ground,i}$ the albedo belonging to the zone's surface without the presence of ice. When the temperature drops below the chosen threshold temperature below which ice forms, here set to 263K, the zone's surface albedo increases from an albedo belonging to an open ocean/ice free land surface albedo to an albedo value of 0.61 belonging to ice. However, the reference surface albedo values used for the two most southern boxes are already higher than the albedo value chosen to represent the albedo of ice. Therefore it is chosen to leave these two boxes out of this feedback mechanism, setting their reference surface albedo values at their default values of 0.63 and 0.84 as can be seen in Table 1.

We have also chosen to implement a second approach for the parameterization of the ice albedo feedback. For this we have followed a method used by Kleidon (2004) who has parameterized the surface albedo as function of temperature according to the fol-

lowing exponential function:

$$\alpha_s = \alpha_{ice,i} - (\alpha_{ice} - \alpha_{s0,i})(1 - e^{-k_s*(T_{s,i}-263)}), \quad (7)$$

where $\alpha_{ice,i}$ represents the albedo of ice; $\alpha_{s0,i}$ the zonal reference surface albedo (see 1) ; k_s a tuning parameter which determines the slope at which the albedo increases with decreasing temperature. This function is applied for zonal surface temperatures ranging from 263 to 273K. Use of this function is supposed to result in a more gradual shift from an ice free zone towards a fully covered zone, in contrast to the previously described method which results in abrupt changes. The first described method for the ice albedo feedback, equation Equation (6), is used throughout the whole research unless specified otherwise.

2.2.2 Cloud and water vapor feedback

Both newly implemented feedback mechanisms, the cloud (Cc) and water vapor feedback (Wv), are parameterized according to the following set of equations:

$$Cc_i = \frac{\exp(a_{Cc}(T_{s,i} - T_{h,i}))}{(1 + \exp(a_{Cc}(T_{s,i} - T_{h,i}))}, \quad (8)$$

$$T_{h,i} = Ts0_i - \frac{\log \frac{Cc_{0,i}}{1-Cc_{0,i}}}{a_{Cc}}, \quad (9)$$

a_{Cc} represents the tuning parameter for the cloud feedback, $T_{h,i}$ the reference surface temperature, and $Cc_{0,i}$ the reference cloud cover. Equation (8) results in a sigmoid relationship ranging between zero and one with increasing temperature, where the variable a_{Cc} determines the steepness of the slope. The equations are now shown for the cloud feedback, but can also be used for the water vapor feedback through replacement of Cc_i, $Cc_{0,i}$, and $a_{Cc,i}$ by Wv_i, $Wv_{0,i}$, and $a_{wv,i}$, respectively. Both feedback mechanisms are parameterized as function of the modeled surface temperature compared to the reference surface temperature as well as the reference values for the cloud cover or water vapor constant.

The water vapor feedback on average causes any potential temperature increase to be doubled or even tripled (Hall and Manabe, 1999; Held and Soden, 2000; Myhre et al., 2013). The tuning factor a_{wv} in Equation (8) and (9) is chosen in such a way, that when the global average temperature increases by one degree in the model, it will be doubled if the water vapor feedback is included within the model run. a_{Cc} is subsequently chosen in such a manner that the model simulation resulted in a numerically stable solution of the system. When the value was set higher, the model setup in which all feedback mechanisms are activated jointly, was unable to reach a stable temperature due to a runaway effect of the cloud cover.

2.2.3 Sensitivity analysis

In order to compare the strength of the feedback mechanisms, we have conducted a climate sensitivity analysis.The climate sensitivity parameter λ was calculated according to:

$$\lambda = dT/dQ, \quad (10)$$

where dT represents the change in temperature between model simulations with no increase in solar constant and with an increased solar constant, and dQ represents the change in radiation between the aforementioned model simulations. To result in λ values for the feedback mechanisms, λ of the model without feedback mechanisms is subtracted from λ associated with the other model setups. These calculations were done for four experiments, in which the solar constant is increased from 1% to 10%.

2.3 *Entropy calculation*

The model has further been extended by including diagnostic calculations of entropy production associated with horizontal heat transport, enabling evaluation of the MEPP. Entropy production was calculated using two different methods, proposed by Paltridge (1975, 1978) and Lorenz et al. (2001).

2.3.1 Paltridge's method

In his seminal paper, Paltridge used Equation (11), to calculate entropy production associated with horizontal heat transport, which is explained more elaborately by Ozawa et al. (2003).

$$S_{hf} = \sum_{i=1}^{18} \frac{F_{out,i} - F_{in,i}}{T_{a,i}}, \quad (11)$$

wherein $F_{in,i}$ represents the net incoming shortwave radiation, $F_{out,i}$ the outgoing longwave radiation at the

top of the atmosphere (TOA), and $T_{a,i}$ the temperature at the TOA which is the systems border at which these fluxes are exchanged with system Earth.

Near the poles, the net incoming radiation is smaller than the outgoing radiation, which results in positive values for entropy production. Conversely, near the equator, the net incoming radiation is higher than outgoing radiation, resulting in negative values for the lower latitudes. Due to the fact that emission temperatures near the equator are higher than those at the poles, a summation of all boxes should globally result in positive entropy production values. Although, as stated by the second law of thermodynamics, entropy production is always positive, this method results in negative values for the lower latitudes. Because of this, a trade off of this method is its inability to calculate zonal values of entropy production, and therefore is only applicable on a global scale.

For calculating the zonal outgoing radiation $F_{out,u}$, Budyko's method was applied:

$$F_{out,i} = A_{n/s} + B_{n/s} T_{s,i}. \tag{12}$$

The absorbed radiation is calculated through

$$F_{in,i} = Q_i(1 - Cc_i\alpha_{c,i})(1 - \alpha_{s,i}). \tag{13}$$

Because the atmospheric temperature is not explicitly considered within Budyko's model, the equation for calculating the temperature at the TOA has been adapted from Paltridge (1975, 1978):

$$T_{a,i} = ((G\sigma T_{s,i}^4(1 - Cc_i) + f\epsilon'\sigma T_{s,i} Cc)/\sigma)^{\frac{1}{4}}, \tag{14}$$

where G represents the fraction of longwave radiation loss to space by a cloud free atmosphere, f a reduction fraction by which black-body radiation from clouds is reduced compared to surface black-body emission due to the lower temperature of clouds, σ the Stefan-Boltzmann constant, and ϵ' the constant of the atmospheric window to IR.

2.3.2 Lorenz's methods

The second method used to calculate diagnostically the entropy production is a slight variation on the method used by Lorenz et al. (2001). The method used by Lorenz et al. (2001) for calculating entropy production associated with meridional heat transport will be applied here, however the manner in which heat transport is calculated here differs from theirs. The equation for entropy production as found in Lorenz et al. (2001) is:

$$S_{hf,i} = F_{hf,i}\left(\frac{1}{T_{s,i}} - \frac{1}{T_{s,i+1}}\right), \tag{15}$$

wherein $F_{hf,i}$ represents the zonal meridional heat flux. Surface temperatures of two different zones are included in the equation. $T_{s,i}$ represents the surface temperature of the cooler box, while $T_{s,i+1}$ is the temperature of the warmer box of the two, i.e. the box from which the heat flux originates.

Lorenz et al. does provide an equation for calculation of the meridional heat flux, which is:

$$F_{hf,i} = k_t(T_{s,i+1} - T_{s,i}), \tag{16}$$

where k_t represents the heat transport constant. However, within the model from Lorenz et al., k_t has a value in the range of 0.6-1.1 W/m^2/K while ours has a default value of 3.81. If Equation (16) would be implemented in our model, it would result in unrealistically large heat fluxes, making its implementation an undesirable choice. Therefore, two other methods were used for calculation of the meridional heat flux.

Basically, when assuming steady-state conditions, $F_{in,i} - F_{out,i}$ can be interpreted as the zonal gain or loss of energy through meridional heat transport. The first manner in which this is calculated here, is by use of Equation (12) and (13). The second manner in which the zonal difference in heat is calculated here, is by use of an empirical relation proposed by Budyko:

$$D = k_t(T_s - T_p). \tag{17}$$

Both approaches for calculating the zonal gain or loss of energy due to meridional heat transport were implemented and compared to determine their implications for entropy production. However, to calculate entropy production according to Equation (15), both methods first have to be converted towards zonal heat flux values. This was done using the simple principle that for each box, the zonal gain or loss of energy through meridional heat transport is equal to energy input minus output.

2.3.3 Entropy maximization

For all three methods, entropy production due to meridional heat transport has been maximized as function of the heat transport constant, k_t. For each method used to calculate entropy production, we have maximized k_t for a model setup wherein no feedback mechanisms were considered as well as for each possible combination of feedback mechanisms activated.

In order to determine which value of k_t results in the highest maximum in entropy production, the simplex method of Nelder and Mead was used (Nelder and Mead, 1965; Lagarias et al., 1998). Afterwards, we compared the k_t values resulting in the highest maximum in entropy production to our model's default value of 3.81 W/m^2/K.

2.4 Snowball Earth implementation

As done by Gerard et al. (1990), we will perform an experiment testing whether constraining the model by MEPP results in a broader range of solar constant values for which the Earth is not in a fully glaciated state compared to an unconstrained model setup. While constraining the heat transport constant by the MEPP, we have slowly decreased the solar constant in our model in steps of 10 W/m^2 until all zones within our model were fully covered in ice. We constrained the heat transport constant by use of all three previously described methods of entropy production.

For comparison, we have likewise decreased the solar constant in steps of 10 W/m^2, however without constraining the heat transport constant but keeping it fixed at its default value of 3.81 W/m^2/K. Afterwards, we compared the percentage needed in solar constant reduction between the three methods for calculating entropy production and with the unconstrained method. Once again, to determine at which value of k_t entropy production reaches its maximum, we used the simplex method of Nelder and Mead (Nelder and Mead, 1965; Lagarias et al., 1998).

3 Model validation

Here we present an evaluation of the model simulations to indicate how well our model captures the most salient features of the Earth's climate system. The observed average planetary temperature and albedo are 287.8K (Hazeleger et al., 2012; Sellers, 1965; Cess, 1976) and 0.315 (Cess, 1976) respectively. The model that was developed in this study simulates a global mean temperature of 287.3K and an albedo of 0.307 when no feedback mechanisms are activated. When all feedbacks are activated, it simulates a global mean temperature of 287.8K and planetary albedo of 0.315, which is remarkably similar to observations, especially when considering the simplicity of the model.

Modeled zonal values of various diagnostic parameters are presented in Figure 2 together with corresponding observed values (Haurwitz and James, 1944; Sellers, 1965) and other model simulation results (Carissimo and Oort, 1985). Here, we show the model's simulated temperature (plots a and b), surface albedo (plot c), cloud cover (plot d), and heat flux (plot e) can be found.

Figure 2a shows the zonal temperature curve for simulations without any feedback mechanisms activated and with a default solar constant of 1370 W/m^2 (dash-dot line) as well as for an increased solar constant of 3 and 10% (dotted lines). Similar to the result for the average planetary temperature, the zonal temperature pattern is in good agreement with observational data (solid line) overall, with just a slight deviation found near the poles which is caused by the reference values used for the surface and cloud albedo and cloud cover in the model. Figure 2b likewise shows the model's zonal temperature curve (dashed line) compared to observed values (solid line), but here each feedback mechanism is activated individually as well as all combined. The model results still agree well with observations.

Zonal surface albedo and cloud cover values from the model are analyzed in Figure 2c and d. It can be seen that like the temperature curve, these too are in good agreement with their corresponding observations (Sellers, 1965), both when solely the individual feedback mechanism is activated as well as when all are considered jointly. Subsequently, the increase in solar constant is used to further check the implementation of the feedback mechanisms. An increase in the model's temperature associated with enhancement of the solar constant should cause ice ablation and thus a lowering of the surface albedo of the corresponding zone. As can be seen in Figure 2c, the implemented ice albedo feedback works as expected, the zones spanning from

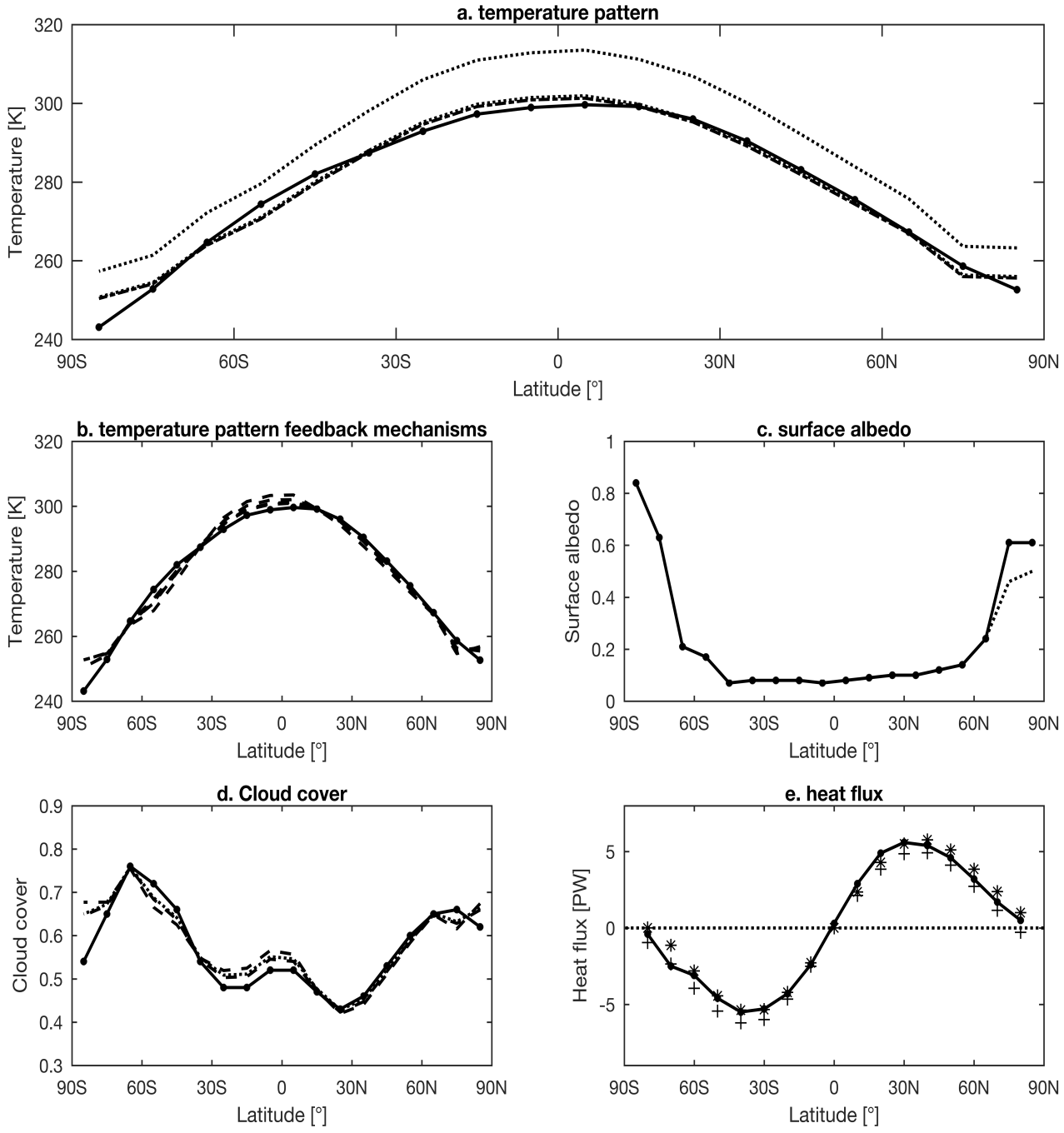

Figure 2: Observed temperature gradient (Haurwitz and James, 1944), surface albedo, cloud cover (Sellers, 1965), and calculated heat fluxes (Carissimo and Oort, 1985) compared to model simulations with default solar constant and with an increased solar constant of 3% and 10%. The dash-dot lines represent the model's simulations without activation of the feedback mechanisms; the dashed lines model simulations with each feedback mechanisms activated separately as well as concurrently; the dotted lines model simulations with either a 3% increase in solar constant or 10%; the plus-signed line represents the heat flux calculated by use of the method from Paltridge (1975); the star-signed line the heat flux calculated by use of the method from Lorenz et al. (2001); and the solid lines represent observational data.

70 to 90 degrees north show a reduced albedo due to the 10% increased solar constant (dotted line). Figure 2c also includes a line where no feedback mechanisms are activated as well as when solely the surface albedo feedback is activated and when all feedbacks operate jointly. However, these lines lie beneath the line representing observational data, causing there to be only one line visible within the graph. This indicates a good representation of the surface albedo within the model simulations (. An increase of the solar constant in our model should also result, besides a lower surface albedo, in a higher simulated cloud cover. Figure 2d displays that this behavior appears to be accurately captured by the model (dotted line). The cloud clover increases in each zone with exception of the southernmost box when compared to model simulations without an increase in solar radiation (both dashed lines).

Figure 2 e shows the calculated zonal heat flux for both methods compared to computed values obtained from Carissimo and Oort (1985). Both in magnitude and pattern, the model simulations agree surprisingly well with observations. The plot does show slight discrepancies between the two methods used, indicating the relevance of calculating the entropy production for two methods. When taking a closer look at the plot, it can also be seen that the line representing the heat flux calculated by use of the method from Paltridge (1975, 1978), becomes slightly negative at the most northern box. This indicates that our model has a slight inconsistency within its energy balance.

Table 2 shows the differences between absorbed shortwave radiation and emitted longwave radiation at the top of the atmosphere compared to values found in literature for several model set-ups. The discrepancy is in the range of -0.6929 to -2.4197 W/m^2, depending on which feedback mechanisms are included. Unfortunately, we were unable to resolve this issue in our model while maintaining values for all variables representative of the current climate. However, the main reason for this unclosed energy balance appears to be the representation of the meridional heat flux in the model. When the value of the heat transport constant (k_t) is set to 0, the model without consideration of feedback mechanisms has a closed energy balance.

The model does not calculate the water vapor content of the atmosphere directly, but solely the concurring radiative effect on the incoming longwave radiation of the system. This implies that we cannot directly evaluate this model feature by comparison with observations. However, as aforementioned, the water vapor feedback tuning parameter was selected such that it would cause a doubling of any surface temperature increase enforced on the system. When we introduced a temperature increase in the model of 3.2 K, by increasing the solar constant with 3%, activation of solely the water vapor feedback resulted indeed in a total global warming of 6.4 K.

4 Model feedback behavior

Here we will analyze the behavior of our implemented ice albedo, cloud, and water vapor feedback also

Table 2: A comparison between absorbed shortwave radiation and outgoing longwave radiation at the top of the atmosphere for several model set-ups and other literature, values are in W/m^2.

Model	Absorbed shortwave radiation	Emitted longwave radiation	Difference
No feedback	236.1876	236.8804	-0.6929
Ice albedo feedback	236.1876	236.8804	-0.6929
Cloud cover feedback	235.8316	237.2272	-1.3956
Water vapor feedback	236.1876	237.2680	-1.0805
All feedback's present	235.3256	237.7453	-2.4197
Trenberth et al. (2009)	239.4	238.5	0.9
Kiehl and Trenberth (1997)	235	235	0
Hazeleger et al. (2012)	242.6	242.7	-0.1
Hartmann et al. (2013)	240	239	0.6

since this enables us to better evaluate and understand entropy production due to meridional heat transport in our model. We have analyzed the model setup in which all feedback mechanisms were considered jointly.

4.1 The ice albedo feedback

Figure 3 shows the simulated global mean surface albedo as function of the heat transport constant (k_t) as well as the global mean cloud cover and water vapor constant. The abrupt changes present in the global average surface albedo can easily be explained by looking at the way in which we implemented the ice albedo feedback in our model. The ice albedo feedback is parameterized according to a simple step function (see Equation (6)) that checks whether the temperature is below a certain threshold in each zone. If the temperature of the box indeed is below the threshold, it is assigned an albedo representative of ice. Otherwise it will keep its original albedo value representative of its surface. Although this is a very rudimentary parameterization of the ice albedo feedback, the same approach has been successfully applied previously by for example Gerard et al. (1990) who used it to test the faint young sun paradox by use of the MEPP. This parameterization of the ice albedo feedback can thus only result in abrupt changes of albedo from either no ice in the zone at all, to the whole zone immediately being covered in ice, largely increasing its surface albedo. It is though interesting to note that there seems to be multiple tipping points and that there is not one major tipping point in which the Earth changes from a state in which it is mostly covered by ice to one state where it is completely ice free, behavior that is observed when using Budyko's model with increasing and decreasing solar radiation.

4.2 The behavior of the Cloud and water vapor feedback

As aforementioned, the average global surface albedo decreases due to ablation of ice. This leads to increased zonal surface temperatures and therefore also leads to an increased cloud cover and water vapor content, see Figure 3. Between the abrupt shifts in cloud cover and water vapor constant, caused by the previously presented abrupt changes in surface albedo, the

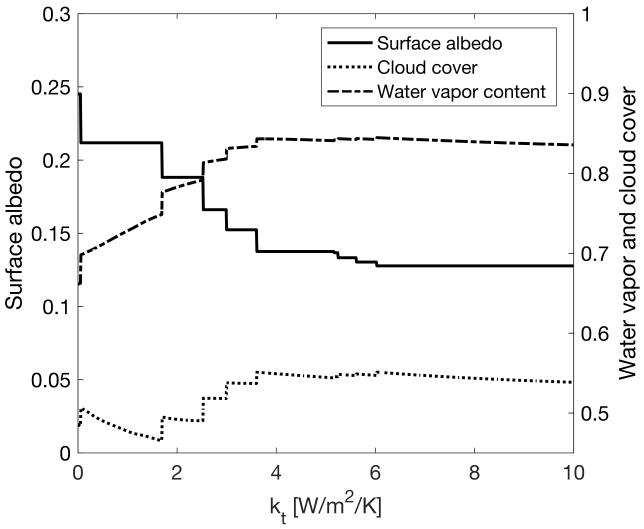

Figure 3: Average global values are plotted for the surface albedo, cloud cover, and the water vapor constant over a range of heat transport constant values, k_t.

cloud cover slightly decreases with k_t, while the water vapor constant slightly increases. The water vapor and cloud feedback are parameterized identically within the model and thus both behave akin (see Equation (8) and (9)). When the surface temperature of a zone increases, e.g. due to enhanced energy transport from warmer to cooler zones due to an increase in k_t, both feedback mechanisms are parameterized to behave similarly, in that both feedback mechanisms should result in an enhancement of the parameter in question. This unforeseen contrasting behavior of the feedback mechanisms presented in Figure 3, can be explained by taking a closer look at the behavior of both feedbacks within the equatorial zones compared to the zones in the polar region.

The dissimilar behavior of the cloud and water vapor feedback can be explained by looking at the reference values used for each feedback mechanisms and how they are parameterized in our model approach. One explanation for the difference in behavior lies in the fact that the cloud feedback uses zonal dependent reference values, while the water vapor feedback uses a global reference value for each zone (as zonal values were not available). However, the difference can to a greater extend be assigned to the locations of the refer-

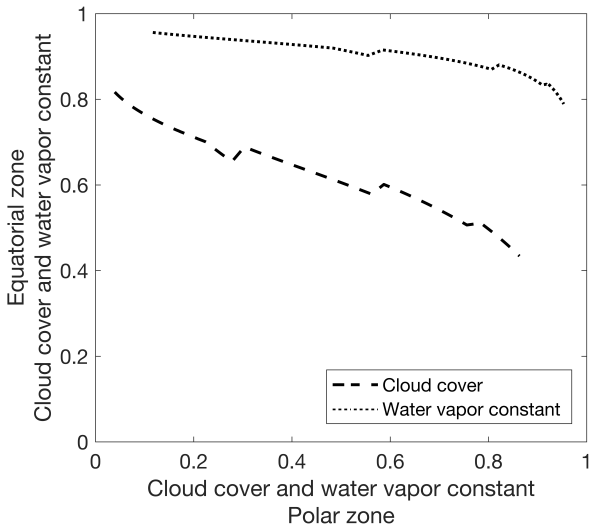

Figure 4: Both cloud cover and water vapor constant values are plotted for a range of k_t values from 0 to 10 in steps of 0.01. Left at the start of the lines, k_t is at a value 0.01, while right on the end, k_t has a value of 10. Cloud cover and water vapor constant values belonging to the zone closest to the equator in our model are plotted against the y-axis, while the values belonging to the most northern box in our model are plotted against the x-axis.

ence values. The difference in behavior between both feedback mechanisms is visualized in Figure 4.

Within Figure 4 we have depicted the cloud cover and the water vapor constant as function of k_t. For variables, the values belonging to the zone in our model closest to the equator are set out against values from the zone closest to the North Pole. As can be seen from the figure, both feedback mechanisms behave rather similarly when solely looking at values belonging to the polar zone, represented on the x-axis. Both the cloud cover and water vapor constant have a value near 0.1 for the polar zone for a k_t of 0, and both end in a similar fashion at a value near 0.9 when k_t has reached a value of 10. When we take a look at the equatorial zone, which is represented on the y-axis, we see a much steeper slope for the cloud cover as function of k_t than for the water vapor constant. The cloud cover ranges from 0.82 to 0.43, while the water vapor constant only ranges from 0.96 to 0.79. The change in equatorial cloud cover as a function of an increase in k_t thus covers a range of 0.39, while the water vapor constant covers a range of only 0.17. These differences in behavior in the equatorial zone can be ascribed to the reference values used in combination with our parameterization method.

To parameterize the cloud and water vapor feedback mechanisms, we used a sigmoid function ranging from 0 to 1 with increasing surface temperature. 0 naturally represents absence of both cloud cover and water vapor in the atmosphere and 1 represents a fully covered atmosphere and a maximum atmospheric water vapor content, with the function's steepest slope and, consequently, the largest impact of the feedback mechanisms is at a value of 0.5. This implies that selection of the actual reference values determines the systems sensitivity to the feedback mechanism. A reference value $>$0.5 implies a reduced sensitivity for the relative warm zones whereas the sensitivity is larger for the cooler zones; a value $<$0.5 results in a larger sensitivity for the warmer zones. The larger the difference between the reference value and 0.5, the smaller the overall feedback sensitivity is.

Table 1 includes the reference values used for cloud cover. The table shows that our reference values for the zones ranging from 0-10° North and 80-90° are 0.52 and 0.62 respectively. As for the reference values of the water vapor constant, both are set to the global average value of 0.8409 (Trenberth et al., 2009). Due to the function's steepest slope being at a value of 0.5, the simulated Earth system is more sensitive to a change in temperature for the cloud cover than it would for the water vapor constant. The consequences are visible in the equatorial region, but due to large variations in surface temperature it does not occur in the polar region. In the polar area, the surface temperature varies to a far greater extend than temperatures in the equatorial zones do, dominating the overall effect the reference values have the water vapor feedback mechanism.

The fact that this dissimilar behavior occurs in the equatorial instead of the polar zones, causes its effects to be much more apparent. Since in our model, the Earth is not divided into zones with equal surface areas, but the zones are determined by latitudinal differences (each of the 18 zones taking up a band of 10°). This method causes the zones in the equatorial region

to be up to a factor 11 larger than the zones in the polar region causing equatorial zones to have much more weight in the calculations of global average values of variables. This creates the occurrence of a slight decrease in the global average cloud cover although it increases to a greater extent in the polar zone than it decreases in the equatorial zone (see Figure 4).

To conclude, both feedback mechanisms appear to ultimately have a different impact on the simulated climate climate in our simple energy balance model. This is caused by the fact that the reference values used for the cloud feedback mechanisms, also selected to agree with other studies and to arrive at a realist simulation of climate, is quite close to the value of 0.5 resulting in the largest climate sensitivity. On the contrary, the reference values for the water vapor feedback are actually substantially larger than 0.5 implying a strongly reduced sensitivity.

4.3 Feedback sensitivities

In order to compare the strength of the feedback mechanisms, we have conducted a climate sensitivity analysis. Results in Table 3 confirm that the cloud feedback is a negative feedback, while the water vapor and ice albedo feedback both are positive feedbacks. Due to the parameterization method used for the ice albedo feedback mechanisms, the feedback was not triggered until a sufficient increase in the solar constant occurred, resulting in calculated values for λ of 0 W/m^2/K for three out of four sensitivity analyses.

Furthermore, it is visible that the water vapor feedback is much stronger than the cloud feedback with a 1% increase of the solar constant. The climate sensitivity for the water vapor feedback typically receives a value of 2.2 W/m^2/K in general circulation models(Cess et al., 1990). Assessing the climate sensitivity of the cloud feedback on the other hand is more complicated as it can result in both positive and negative feedbacks (Cess et al., 1990), making a direct comparison with literature difficult. However, as the solar constant increases it can be seen that the strength of the water vapor feedback in our model decreases, while the strength of the cloud feedback conversely increases with the solar constant. This pattern though is mainly caused by a decrease in the climate sensitivity parameter belonging to the model setup in which no feedbacks were considered, i.e. is solely influenced by the inherent Stefan-Boltzmann's feedback. For our current model it is fair to say that the water vapor feedback seems to be stronger than the cloud and ice albedo feedback.

Table 3: Results of the climate sensitivity analysis. Values are in W/m^2/K.

Feedback mechanism activation	Solar constant increase 1%	2%	3%	10%
None	3.86	3.50	3.39	3.31
Cloud	1.38	1.64	1.71	1.89
Water vapor	-2.26	-1.87	-1.74	-1.17
Ice albedo	0	0	0	-0.17
All	-1.04	-0.40	-0.17	0.20
λ	2.98	3.26	3.37	3.87

5 Maximizing entropy production

In our Budyko-based model, we have maximized entropy production with respect to the energy transport constant (k_t) in order to test the MEPP. Figure 5 shows entropy production calculated with our model by use of our three described methods as function of k_t when no feedback mechanisms are considered. The first method consists of entropy production due to meridional heat transport calculated as proposed by Paltridge (1975, 1978); in the other two methods, entropy production is calculated by use of the method proposed by Lorenz et al. (2001). The second method was subsequently split up in two alterations, which from now on will be referred to as Lorenz P and Lorenz B. In Lorenz P, the heat flux needed to calculate entropy production is inferred from the zonal difference in incoming shortwave radiation and outgoing longwave radiation and which is mainly based on Paltridge's method. In Lorenz B, the heat flux is inferred from the zonal difference obtained from an empirical relation proposed by Budyko (1969). Table 4 subsequently shows the values of k_t acquired by optimization of entropy production in our model where either no feedback mechanisms are considered and for each possible combination of activated feedbacks.

In our model a k_t value of 3.81 W/m^2/K, as used within Budyko's original model, results in the best agreement for the current climate. As can be seen in

Table 4, maximization of entropy production for each of the three methods, without consideration of feedback mechanisms, results in k_t values in the range of 2.02 to 2.23 W/m^2/K. Application of a k_t value in that range would result in too low of a heat flux in our model, and subsequently in temperatures that are too high in the tropics and too low in the temperate region. It is however note worthy that, as can be seen in Figure 5, the three applied methods result in identical behavior of entropy production as a function of k_t. Besides, basically the same pattern in entropy production was presented by Lorenz (2002, 2010) in which no feedback mechanisms were considered either.

It was expected that at least part of the obtained values for k_t would be comparable to the previously mentioned optimal value of 3.81 W/m^2/K for our model. This was expected in particular to be true for k_t values corresponding to the model with no feedback mechanisms included or solely the ice albedo feedback, as results of previous studies have indicated so (e.g., Paltridge, 1975, 1978; Grassl, 1981; Wyant et al., 1988; Gerard et al., 1990; Lorenz et al., 2001; Kleidon, 2004, 2010; Pascale et al., 2012). Table 4 however shows that, with exception of one simulation (for which paltridge's method was used and included all feedback mechanisms), the k_t values obtained by maximizing entropy production in our model clearly disagree with a value that would allow for a good representation of the current climate.

One interesting and perhaps important observation is that the use of one global value for the heat transport constant results in underestimated temperatures at the lower latitudes while overestimating the temperature at higher latitudes (Lorenz, 2002). It would be interesting to test whether the MEPP is able to successfully reproduce the current climate while using zonally differing heat transport constants in Budyko's or another comparable model. In principal this also is what Paltridge has done; he avoided the use of a heat transport constant by working directly with the unknown zonal heat fluxes.

5.1 Model setup

Golitsyn and Mokhov (1978) (as cited in Wyant et al., 1988) used a Budyko-Sellers type of zonal energy balance model, comparable to the model used here, to test

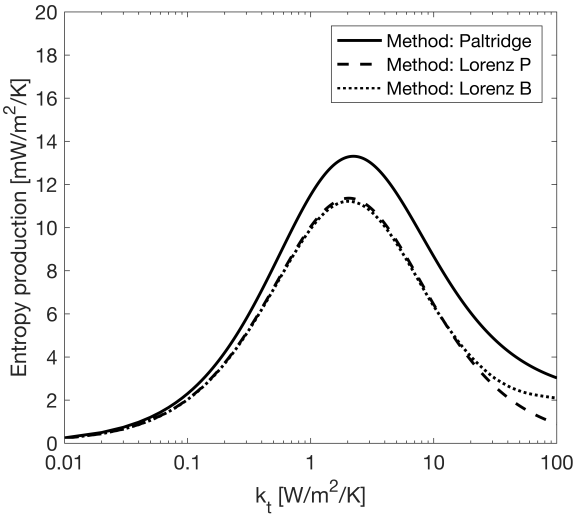

Figure 5: Entropy production as function of the heat flux constant, k_t, plotted for the three methods used in this study when no feedback mechanisms are considered.

Table 4: k_t values in W/m^2/K corresponding to the highest maxima in entropy production in our energy balance model. Values are obtained for the model with either no feedback mechanism considered as well as for each possible combination of activated feedbacks. Methods by Paltridge (1975, 1978) and by Lorenz et al. (2001) are used for calculation of entropy production, in which the method by Lorenz et al. is divided into two variations. B is the method in which heat transport is calculated by use of Budyko (1969), while in P, Paltridge (1975, 1978) was used. Corresponding values of entropy production can be found in Table 5.

Feedback mechanism activation	Paltridge	Lorenz B	Lorenz P
None	2.24	2.03	11.4
Cloud	1.92*	4.39*	9.7*
Water vapor	2.72*	1.67*	10.4
Ice albedo	1.28*	1.28*	15.7*
Ice albedo & cloud	2.94*	1.18*	9.3*
Ice albedo & water vapor	5.84*	1.22*	19.6*
Cloud & water vapor	1.81	1.88*	9.5
All	3.62*	1.50	14.1*

** Indicates the presence of multiple maxima.*

the MEPP. Their results also showed that the energy transport constant obtained through maximization of entropy production does not agree well with empirical estimates. They concluded from their results that the MEPP is not applicable to simple climate models. On the one hand, results obtained in our study seem to substantiate their conclusion, but on the other hand they have no added value because the same model was used as basis in our study as was used in theirs. This could mean that Budyko's model contains certain features that limit application of this system to further asses MEPP. As previously mentioned, multiple other studies that used simple climate models were able to reproduce the current climate when their model was constrained by the MEPP. Differences in model setup could thus be explanatory for the dissimilarity in results found between several studies that applied the MEPP to simple energy balance models.

Let us take the model set-up of Paltridge (1975) as an example, as he was able to successfully reproduce the current climate by constraining his model by the MEPP. Paltridge developed a simple 10-box energy balance model spanning the entire globe, assuming a closed energy balance for each box. His model was set up in such a manner that there are basically three unknowns present, namely: temperature, cloud cover, and heat tranport. In principle, this leads to an unsolvable model. However, constraining the heat flux by the MEPP enabled him to reproduce, surprisingly accurately, not just the current average temperature but also the cloud cover and heat flux for each box. Our model on the other hand, in its most basic form consisted of an already complete model, with the ability to accurately represent the current climate. In short, Paltridge developed an incomplete model that needs a constraint like the MEPP to be able to solve the calculations of energy balance, transport and resulting temperature distribution, while we adapted a valid existing model to test the MEPP. This possibly led to overspecification of certain variables and constants in our model. A different explanation could be the choice of inaccurate starting values, which potentially has large repercussions in the system due to the presence of many parameterizations of processes. A more detailed study on the relation between model setup and entropy production is needed in order to determine with certainty how a varying model setup influences the outcome.

5.2 Time dependence

Wyant et al. (1988) have indicated a model characteristic which, according to them, is essential for successful application of the MEPP in simple climate models. Their study namely concluded, that inclusion of a time dependent radiation source, e.g. consideration of a seasonal cycle in radiation, is essential to successfully apply the MEPP. This provides an interesting model characteristic that could enable a successfully application of the MEPP in simple climate models, but they were unable to provide a theoretical foundation why consideration of this seasonal cycle in radiations would allow the model to result in a state of maximum entropy production. This however, does propose an explanation as to why application of the MEPP perhaps was not as expected in our study. Would we have known from the start, it could have been implemented here as well based on studies by North and Coakley Jr (1979) and Su and Hsieh (1976) for example. Although, using a simple two-box energy balance model, we were able to test the effect of this proposed role of seasonality in incoming radiation on the application of the MEPP. This model includes the possibility to switch seasonality off and on as needed. Details of this model and its implementation can be found in Appendix B.

Figure 6 shows the results of our two-box energy balance model constrained by the MEPP. The simulated temperatures for the equatorial and temperate box are shown as a function of the transport constant (k_t). The Figure also includes entropy production due to meridional heat transport which is shown for the model with and without consideration of the seasonal cycle in radiation. Besides entropy production, the temperatures are also plotted for the model with and without the seasonal cycle activated, although these differences are too small to visualize in such a manner. Nonetheless, that there are differences in temperature between the simulations with and without seasonality in radiation can be inferred from the differences in entropy production, as entropy production directly depends on temperature.

The vertical lines in Figure 6 indicate the peaks

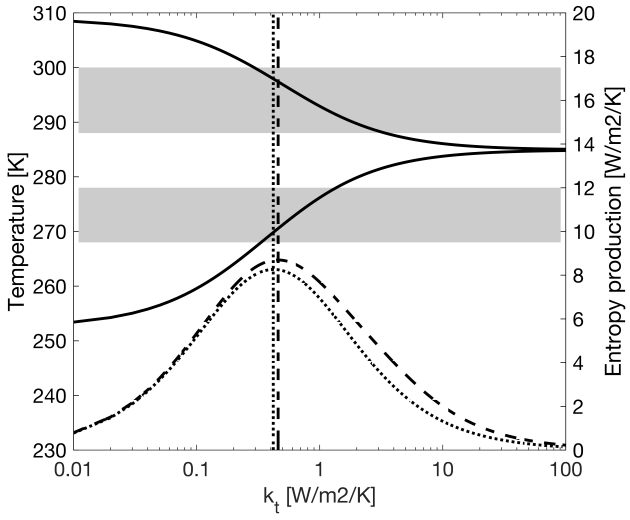

Figure 6: Shown is the modeled temperature of the two-box model as a function of the heat transport constant. The upper solid line represents the equatorial box; the lower the temperate box; and the shaded areas a range of observed values in these two regions. At the bottom of the graph entropy production is plotted for the model with seasonality activated (dashed line) as well as with seasonality switched off (dotted line). Figure and observed values after Lorenz et al. (2001)

of entropy production. The inclusion of seasonality appears to result in a slight enhancement in entropy production at a slightly larger k_t value but also seems to result in zonal temperatures slightly closer towards the middle of the banded areas representing observed temperatures. Consideration of seasonality thus causes the model to move, although slightly, towards a more realistic representation of the current climate.

The influence of seasonality within the model seems rather small when looking at Figure 6. However, in light of the fact that these two boxes represent the whole of the Northern hemisphere within a simple model, it can be argued that its influence potentially is larger when applied to models with increasing complexity and detail. Inclusion of seasonality in a model when studying the MEPP thus potentially poses an important and at least interesting phenomenon. In future research on the MEPP when using both simple energy balance models and more advanced models, seasonality, e.g. consideration of a seasonal cycle in radiation, should be included in the model to explore its effects in greater detail.

6 The existence of multiple maxima

Paltridge (1975, 1978) has noted that there is no prove to be found for the presence of multiple maxima in entropy production in his model. One main reason for not having such multiple states of maximum entropy production is probably the lack of feedback mechanisms in his model. Figure 7 shows how entropy production due to meridional heat transport in our model behaves as a function of the heat transport constant, k_t, when all feedback mechanisms are activated jointly. It is clearly visible that, in our model, there are multiple local maxima in entropy production for two of the three methods, specifically those from Paltridge and Lorenz P. When looking at the entropy production calculated by use of Paltridge's method, it can even be seen that there are peaks representing nearly identical values of entropy production but consisting of differing values for k_t. Although the method from Lorenz, in which the heat flux is determined by use of Budyko's method, does not show multiple peaks, the same broad pattern is present.

Figure 5 depicts the behavior of entropy production in our model when no feedback mechanisms are considered. It showed how strikingly similar the behavior of entropy production between each of the three different methods is in our model. If we now look at entropy production for each of the three methods in Figure 7, we see that the behavior has become quite dissimilar. Although all three methods are proposed to calculate the same, namely entropy production due to meridional heat transport, they each result in quite different values and behavior with an enhancement of the model's complexity. A possible reason for this is that our model's energy balance is not entirely closed as seen in Table 2. Entropy production calculated by Paltridge's method for example, is highly dependent on the zonal values of absorbed shortwave radiation and emitted longwave radiation. Any inconsistency present in these variables could thus have considerable repercussions for our calculated values of entropy production.

For a more detailed analysis of what actually explains the simulated behavior in entropy production as

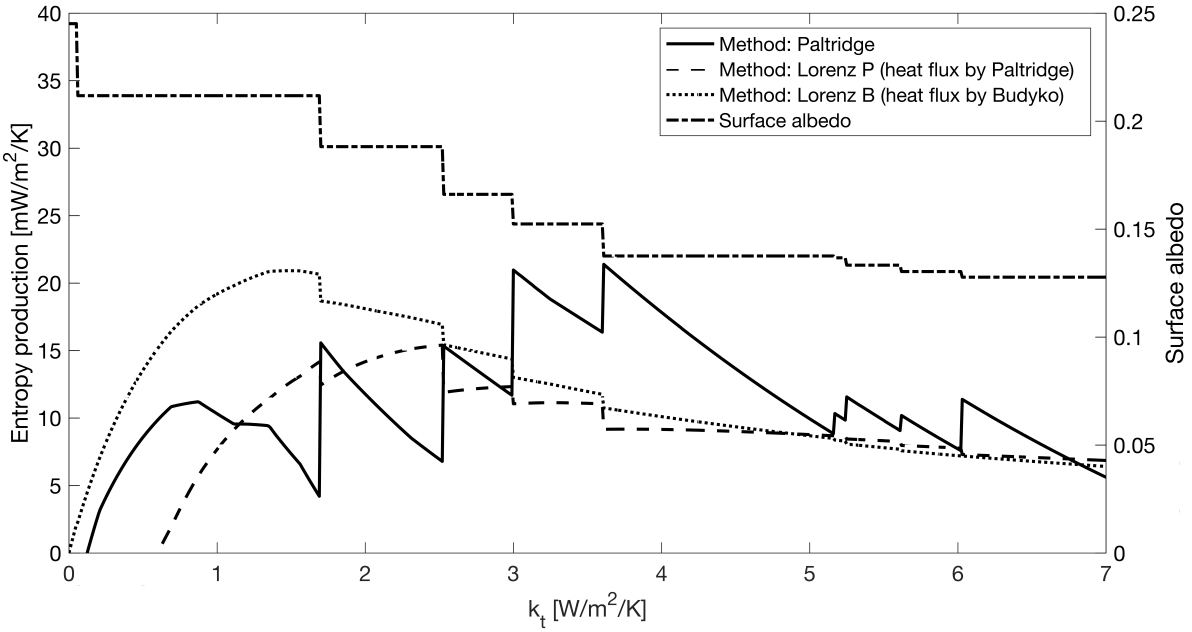

Figure 7: Entropy production with all feedback mechanisms activated jointly is plotted as function of the heat transport constant. Next to that is the global average surface albedo plotted against the right axis.

a function of k_t, we have chosen to focus on one of the three methods used to calculate entropy production. As Paltridge's method was likewise used in a model consisting of multiple boxes representing the entire world, we have chosen to solely focus on that method in the remaining part of this chapter.

6.1 Local maxima

Model setups that resulted in multiple local maxima are highlighted in Table 4 and Table 5 by * behind the values. As these tables show, most model setups which consider either one or multiple feedback mechanisms show the presence of multiple maxima in entropy production as a function k_t. As depicted in Figure 7 the local maxima perfectly align with the drops in the average global surface albedo. This simple but clear interaction indicates the immensely important role of the ice albedo feedback for entropy production maximization within our model. In our model implementation, the ice albedo feedback seems solely responsible for the existence of multiple local maxima in our model. However, one has to wonder how realistic this representation of ice cover within the model is.

The number of zones within the model has a large influence on how the feedback mechanism operates to a large extent. The feedback causes whole zones within the model to be either fully covered in ice or that there is no ice present at all. The feedback can thus operate more freely within a model containing a large number of zones, allowing it to glaciate smaller surface areas of the world at a time. Lian and Cess (1977) have re-examined the role of the ice albedo feedback within zonally average energy-balance models. They found that especially Budyko's model appears to substantially overemphasize the influence the ice albedo feedback should have on the Earth's climate. Their analysis showed that the ice albedo feedback sensitivity parameter in Budyko's model is a factor six too large.

Because of the current restriction in surface albedo and its potentially falsely perceived importance when using the current parameterization in the model, we have chosen to perform the same tests, while implementing a different approach to represent the ice albedo feedback. This was done by use of our second described method for the ice albedo feedback parameterization. This method uses an exponential function,

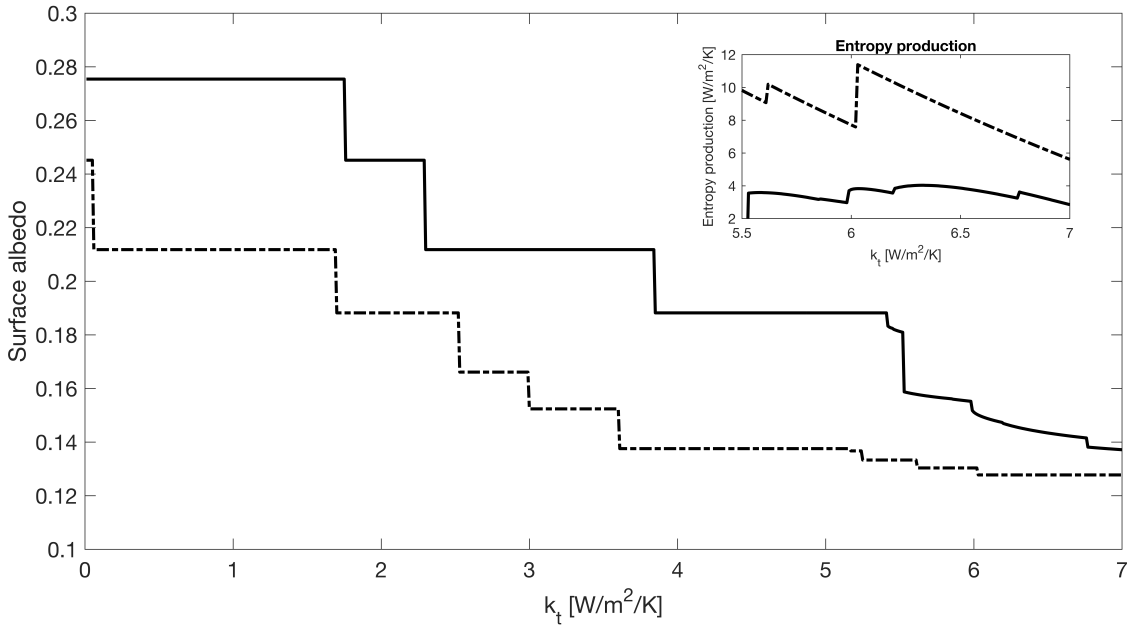

Figure 8: The global average surface albedo is plotted as function of the heat transport constant, k_t, for the model with the ice albedo feedback calculated by use of the step-function, as well as for the model that uses the exponential function. In both model setups, all feedback mechanisms were activated jointly. For k_t values in the range of 5.5-7 an inset of entropy production is also shown for both model setups.

given in Equation (7), instead of the step function that was given in Equation (6). The impact of this alteration in our model on entropy production and surface albedo is displayed in Figure 8.

Figure 8 depicts the change in the global mean surface albedo as function of k_t for both parameterizations of the ice albedo feedback. For most boxes, the shift from no ice to full ice coverage still occurs instantly in our model. This indicates that once in a certain box starts ice starts to form, increasing its surface albedo, it often does not reach a steady state before it is fully covered by ice or vice verse, as our model is an equilibrium model and only presents steady-state solutions of the system. This effect also has as a consequence, that when k_t is nearly 0, our model with the ice albedo feedback parameterized according to the sigmoid function results in an overall larger ice cover within the system than when parameterized according to the stepwise function. As a result, the model is unable to represent the current climate when using the exponential function. When k_t surpasses a value of 5 W/m^2/K however, the simulated shifts in surface albedo become more gradual in nature. This could be due to the fact that the surface temperature varies less as function of k_t for higher values of k_t. Next to the surface albedo, Figure 8 also shows an inset of the entropy production for both model setups, for k_t values ranging from 5.5 to 7.0 W/m^2/K. This shows, that when the ice albedo changes less sudden, entropy production also changes more gradually, but also that there are now even more local maxima to be found in the entropy production rate. Results of another study confirms this more gradual change of entropy production as function of k_t (Herbert et al., 2011). These results indicate how solely the ice albedo feedback can determine if and where local entropy production maxima exist within our model. When studying entropy production, the behavior of the ice albedo feedback proves to be a critical component of our energy balance model.

Other literature on the MEPP also shows that consideration of the ice albedo feedback tends to show the existence of multiple local maxima in entropy production (Herbert et al., 2011). Besides the mere presence

of multiple maxima, it has even been suggested that the steady-state in which a system finds itself, is not necessarily a state representing the highest maximum entropy production. The state of the system could just as well represent one of the other lower local maxima in entropy production. It implies that in which of the local maxima the system will find itself dependents on initial conditions of the system in question (Herbert et al., 2011).

Noda and Tokioka (1983) studied the MEPP applied to a model with varying distributions of water vapor. Their model also showed that multiple maxima in entropy production exist. One of the states represented a maximum in entropy production and resembled a quite accurate simulation of the current climate. However, this maximum did not correspond with the highest maximum in entropy production but represented one of the lower local maxima.

A study on entropy production in relation to the thermohaline circulation by Shimokawa and Ozawa (2002), found multiple equilibria in their model when constrained by the MEPP. They found that the final steady-state of their system did not necessarily depend on the highest maximum in entropy production, but rather was determined by perturbations introduced into the system. Perturbations either caused the system to irreversibly increase its entropy production, or caused the system to recover to the state it was in before the perturbation occurred. The magnitude and direction of the perturbations introduced in the model were found to be the key factor determining the evolution of the system.

These results seem to indicate that the entropy production provides an indication in which direction a system will evolve over time when disturbed, rather than enabling us to determine the current state of a system by solely looking at maximization of entropy production. An extensive review by Martyushev and Seleznev (2006) also concluded that the MEPP is an indication of the most probable state instead of the current state. However, he did note that if a state of lower entropy production is acknowledged, it concerns a metastable state.

As long as we did not include feedback mechanisms in our model, there is no indication that multiple maxima in entropy production exist, as was indicated by Paltridge (1978). However, consideration of feedback mechanisms in the model runs resulted, for most of the possible combinations of feedbacks, in multiple maxima in entropy production as shown by other studies (Noda and Tokioka, 1983; Shimokawa and Ozawa, 2002; Jupp and Cox, 2010; Herbert et al., 2011).

6.2 Entropy behavior

The presence of abrupt peaks in entropy production can solely be ascribed to the ice albedo feedback. To also explore the behavior of entropy production as a function of k_t between those peaks in entropy production we need to consider the role of the cloud and water vapor feedback globally as well as their zonally differing behavior. As explained in subsection 4.2, although both feedback mechanisms are parameterized identically, they can behave slightly different in each zone because the behavior of the parameterization method differs with the use of different reference values.

In order to fully grasp the behavior of entropy production between the peaks, it is important to determine how entropy production is calculated according to Paltridge's method in Equation (11). When we take the current climate as example, the net incoming radiation is higher than the emitted longwave radiation at the equator. Conversely, near the poles the emitted longwave radiation is higher than the net incoming radiation. From Equation (11) we can subsequently deduce that the difference in emitted versus absorbed radiation results in positive entropy production values near the poles, and in negative values near the equator. The key component that causes the overall entropy production to be positive, is the atmospheric temperature. Atmospheric temperatures are lower at the poles than at the equator, hence positive values of entropy production at the poles should outweigh the negative values seen at the equator. The shown behavior of Equation (11) emphasizes the importance of the zonal behavior of the model in order to analyze the behavior of entropy production due to meridional heat transport. For our explanation of the influence of surface albedo on entropy production, we did use global values of surface albedo. This can however be condoned by the fact that each drop seen in the global surface albedo is caused by a single zones becoming ice free while all other zones remain the same. In order to ex-

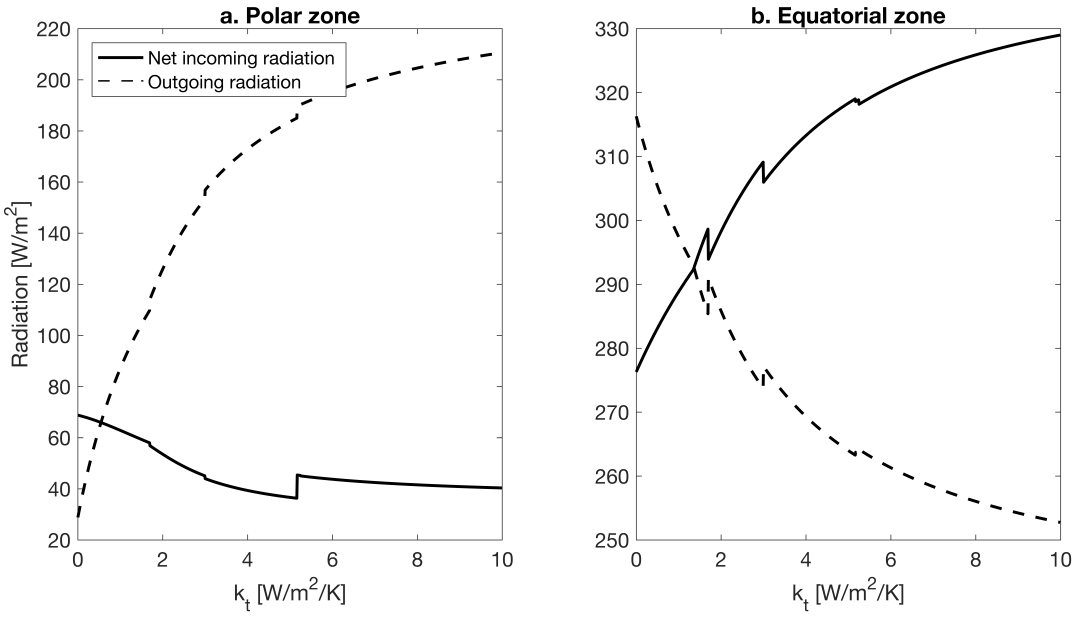

Figure 9: The absorbed radiation with the emitted radiation as function of the heat transport constant (k_t) is shown for the zone closes to the North pole in plot A, and for the zone closes to the equator on the northern hemisphere in plot B. The radiation values are plotted for a model setup in which all feedback mechanisms were considered jointly.

plain the decrease in entropy production between the abrupt peaks according to Paltridge's method, we need to explore zonal rather than global variations in the cloud and water vapor feedback mechanisms within our model.

In Figure 9 we show the absorbed and emitted radiation as a function of k_t for the zone closest to the North Pole as well as for the zone closest to the equator on the northern hemisphere. The polar zone shows a strong increase in the outgoing radiation as function of k_t, together with a slight decrease in the incoming radiation. The latter response reflects the change in the zone's albedo due to the change in cloud cover as well as the change in ice for the simulated change in temperature. If we apply the observed behavior of the radiation fluxes to Equation (11), we can deduce that entropy production in the polar zone as function of k_t increases. However, the increase in entropy production is slightly dampened by the enhanced temperature in this zone, which can be deduced from the increase seen in outgoing radiation as this directly depends on temperature (see Equation (12)). Hence, Figure 9a shows us that entropy production slowly increases in the polar zone of our model with an increase in k_t.

focusing on the equatorial zone, depicted in Figure 9b, we see contrasting behavior in the radiation fluxes. Here, the net incoming radiation strongly increases while the outgoing radiation strongly decreases for an increase in k_t. Application of this behavior to Equation (11) shows how entropy production within the equatorial zone becomes more negative with increasing k_t. Entropy production becomes even more negative due to a decreasing temperature, as deduced from the outgoing radiation. Figure 9B thus shows how the negative entropy production in the equatorial region decreases further with an increase in k_t.

The reason why entropy production decreases for an increase in k_t in between the maxima, can by explained by taking a look at the behavior of both the cloud and water vapor feedback. As shown in Figure 4, the cloud cover strongly increases in the polar zone as function of k_t, resulting in an increase in the albedo of the polar zone. The decrease seen in net incoming radiation in the polar zone reflects an albedo

increase due to the cloud cover feedback. The feedback is thus responsible for the decrease in net incoming radiation as function of k_t, herewith enhancing the rate at which the net incoming radiation diverges from the outgoing radiation with increasing k_t. The increasing water vapor constant augments the rate of increase in outgoing radiation by trapping more heat, resulting in raised temperatures. Both feedbacks enhance the rate at which the differences between the outgoing radiation and net incoming radiation of the polar zone diverge as function of k_t. Hence, the entropy production increase in the polar zone with an increase in k_t is enhanced by both the cloud and water vapor feedback mechanism. This is the first step of the analysis of how the global entropy production decreases as function of k_t (see Figure 7). For a full picture we also need to assess what happens to the radiation balance within the equatorial zone.

Figure 9b shows the opposite behavior in the equatorial radiation fluxes compared to the polar zone.

It can be inferred from Figure 4 that within the equatorial region, Figure 4 both the cloud cover and the water vapor constant decrease with k_t, although the decrease in water vapor constant is less compared to that of the decrease in cloud cover. As for the polar zone, the increase in net incoming radiation mainly reflects the role of the cloud feedback, which enhances the divergence of the radiation fluxes as function of k_t. The rate of decline of the outgoing radiation being the result of our induced increase in heat flux by incrementation of k_t, is enhanced by the reduction of the water vapor constant as function of k_t. Both feedbacks thus enhance the rate at which the radiation fluxes diverge from each other, but for this zone resulting in a stronger decrease in entropy production as function of k_t. If we combine this with the increase in entropy production of the polar zone, this overall results in a global decrease in entropy production with an increase in k_t until the next tipping point on ice formation is being reached.

This further detailed analysis based on Figure 9a and b shows how entropy production increases in the polar zone while further decreases in the equatorial zone as function of k_t. Furthermore, the different behavior of the cloud feedback compared to the water vapor feedback as seen in Figure 4 seem on the one hand to enhance the increase in entropy production in the polar zone with an increase in k_t, while on the other hand the feedback mechanisms more strongly reduces entropy production in the equatorial zone. Besides the effect of the feedback mechanisms on radiation is their influence on temperature also important resulting in an increase in the temperature in the polar zone, while the equatorial zone's temperature further decreases. This effect on the temperature reduces the total entropy production of the system. One important last aspects that has not yet been discussed, is the differing zonal surface area. Our model uses zones spanning 10°rather than zones of equal sizes. Thus although both feedbacks enhance the patterns seen in both the polar and equatorial zone, due to the size being a factor six larger in the equatorial zone, the influence of the feedbacks there is more substantial. This effect can be seen in 9 by the more responsive radiation patterns in the equatorial region compared to the polar region. The cloud and water vapor feedbacks thus enhance the rate at which the radiation fluxes diverge, herewith enhancing the rate at which entropy production increases in the polar zone while also enhancing the rate at which entropy production decreases in the equatorial zone. However, due to the additional effects on temperature as well as the increased weight in the equatorial region resulting from its larger surface area, the rate at which the total entropy production decreases as function of k_t is enhanced by our implemented feedback mechanisms within Budyko's energy balance model.

A last note, Figure 9 also substantiates the peaks in entropy production, as previously discussed, caused by the ice albedo feedback. The abrupt shifts in radiation in the figure perfectly align with the abrupt drops in surface albedo as seen in Figure 7. These abrupt shifts especially manifest themselves in the equatorial region, i.e. the region that entails the largest impact on the total entropy production. The abrupt peaks in radiation in the equatorial region, result in a convergence of the radiation fluxes in the equatorial region, which according to Equation (11) will result in a less negative entropy production. Besides that, the increased outgoing radiation indicates that the temperature also increases, which as well results in a less negative entropy production in the equatorial region. The fact that the drops in albedo result in a convergence of the ra-

Table 5: Values of entropy production due to meridional heat transport in mW/m^2/K representing the highest maxima in entropy production from our energy balance model. Values are obtained for the model with either no feedback mechanism activated as well as each possible combination of feedbacks activated. The method by Paltridge (1975, 1978) and by Lorenz et al. (2001) are used for calculating entropy production, with the method from Lorenz et al. divided into two variations. B is the method in which heat transport is calculated by use of Budyko (1969), while P by use of Paltridge (1975, 1978). Corresponding k_t values can be found in Table 4.

Feedback mechanism activation	Paltridge	Lorenz	
		B	P
None	13.3	11.2	11.4
Cloud	19.3*	9.5*	9.7*
Water vapor	23.1*	24.5*	10.4
Ice albedo	21.4*	12.8*	15.7*
Ice albedo & cloud	17.3*	11.8*	9.3*
Ice albedo & water vapor	25.1*	31.2*	19.6*
Cloud & water vapor	37.7	13.7*	9.5
All	21.4*	20.9	14.1*

** Indicates the presence of multiple maxima.*

diation fluxes in Figure 9b and due to the increased temperature, the entropy production of the system is less negative and thus results in the peak values of entropy production as seen in Figure 7. Even more importantly, as can be seen from Figure 11, without this effect of the cloud and water vapor feedback on the radiation balance, the drops is surface albedo would cause a drop in entropy production. The occurrence of all three feedback mechanisms simultaneously are thus needed in order to result in the peaks in entropy production as seen in Figure 7.

7 Augmented maximum entropy production

A last observed feature of our model is the increase seen in the values representing the highest maximum entropy production when one or multiple feedback mechanisms were considered within the model setup. Table 5 contains the values of entropy production belonging to the corresponding k_t values found in Table 4. We have also visualized this in Figure 11, which shows entropy production within our model as function of k_t for a model setup in which no feedbacks are considered as well as for model setups considering each feedback mechanism separately. The figure clearly shows that model setups considering one of the feedback mechanisms result in a higher peak value of entropy production compared to the model setup considering no feedback mechanisms.

Entropy production values for each method when no feedback mechanisms were considered are in the same order of magnitude as reported in other studies (Paltridge, 1978; Peixoto et al., 1991; Pujol, 2002; Pascale et al., 2012), but generally being slightly larger compared to those studies. For example, Paltridge reported an entropy production of 8.9 mW/m^2/K. It has been raised that entropy production increases as the model's resolution increases up until a certain point Kleidon et al. (2003). The difference in entropy production could result from the fact that our model resolution is slightly higher than that of Paltridge for example, who used 10 boxes. Additionally, the two-box model developed to determine the influence including seasonality has on entropy production, resulted in lower values for entropy production. Namely, the model setup excluding seasonality resulted in an entropy production of 8.26 mW/m^2/K, whereas the setup including seasonality resulted in 8.69 mW/m^2/K, providing additional prove for the link between model resolution and entropy production.

In Figure 10 we have depicted zonal entropy production values according to Paltridge's method belonging to the highest maximum in entropy production, i.e. belonging to k_t values given in Table 4. We have plotted entropy production values for a model setup in which no feedbacks were considered at all, as well as when the model setup contains each of the three feedbacks separately. When the model setup contains a feedback mechanism, we clearly see a less negative entropy production in the equatorial region and a slightly reduced entropy production in the polar regions. The only exception to this is the model setup in which the ice albedo feedback is activated, which results in an enhanced entropy production in the polar region. Note that entropy production values have already been recalculated to take into account the differ-

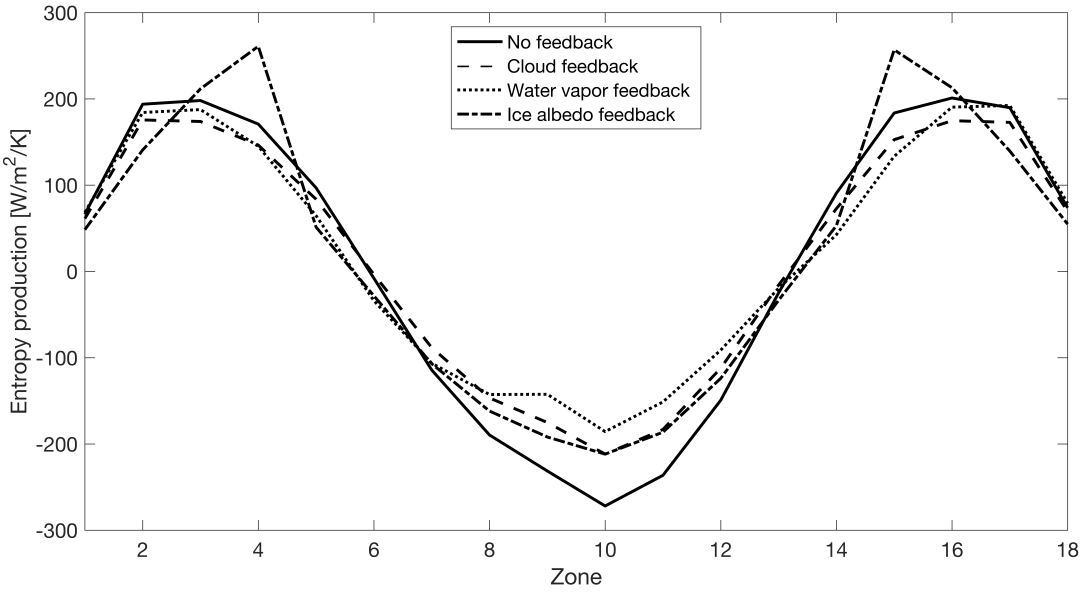

Figure 10: Zonal entropy production values for a model setup in which no feedback mechanisms were considered at all, as well as for model setups considering each feedback mechanisms separately. Entropy production values have been scaled to the zonal surface area.

ing zonal surface areas. In order to explain the behavior seen in entropy production in the different zones, we again have to look how Paltridge's method calculates entropy production. For a detailed description of this function, we would like to refer you to subsection 6.2 and Equation (11).

7.1 Feedback behavior

An explanation as to why entropy production is less negative in the equatorial zone, shown in Figure 10, has to do with the effect of the cloud and water vapor feedback on the radiation balance. As depicted in Figure 4 the cloud cover is high in the equatorial zone for small values of k_t ($<\sim 5$). A higher cloud cover causes an increase in the zonal albedo and thus lowers the net incoming radiation. As can be deduced from Equation (11), lower net incoming radiation in the equatorial zone results in a higher entropy production, i.e. less negative. Note, this seems to contradict observations made in subsection 6.2, where we presented that consideration of both the cloud and water vapor feedback mechanisms resulted in a stronger decrease in entropy production (more negative) as function of k_t. However, there we intended to highlight that for an increase in k_t there is a stronger divergence of the net incoming and outgoing raidiation fluxes, whereas here we want to stress that considering the feedback mechanisms causes the absolute entropy production to increase (become less negative) in the equatorial zone.

In the model setup containing the water vapor feedback, differences in radiation also reduces due to inclusion of the feedback. As depicted in Figure 4 we see an enhanced water vapor constant for the equatorial region when k_t is low. The enhanced water vapor constant causes the atmosphere to trap more heat and subsequently increases the outgoing radiation. As a reduced net incoming radiation does, an enhancement in the outgoing radiation also results in a less negative entropy production according to Equation (11). The feedback mechanisms themselves thus cause the entropy production to be less negative in the equatorial region by enhancement of either the cloud cover or the water vapor constant.

If we apply the same line of thought to the polar/temperate region, we can see from Figure 4 that both the cloud cover and water vapor constant are re-

duced for low values of k_t. Here, the reduced cloud cover and water vapor values result in higher net incoming radiation and lower outgoing radiation respectively. When applying these observations to Paltridge's method in Equation (11), we can deduce that this results in decreased entropy production values for the model setups containing either of the two feedbacks.

For the model containing the ice albedo feedback, it looks like entropy production is enhanced in the polar/temperature region. However, when we sum up the values of zone one up until zone five, it results in a lower entropy production compared to that of the model without feedback mechanisms considered. The radiation balance for all of these five zones resemble the behavior seen in the left plot of Figure 9. In general, as k_t increases, the heat transport in the model increases as well, and subsequently causes zones to become ice-free. As zones become ice-free within the model, the albedo of the zones in question decrease significantly. The reduced surface albedo in the zones then cause an increase in the net incoming radiation. As seen from Equation (11), a higher net incoming radiation results in a reduction of the entropy production. However, this described behavior follows a fine line between either reducing entropy production or increasing it. A second consequence of the reduced surface albedo and increased net incoming radiation, is an enhanced temperature and strong redistribution of the zonal heat fluxes. These alterations result in higher outgoing radiation levels in certain zones and thus in a higher entropy production, as can be seen by the two peak values in Figure 10 as well.

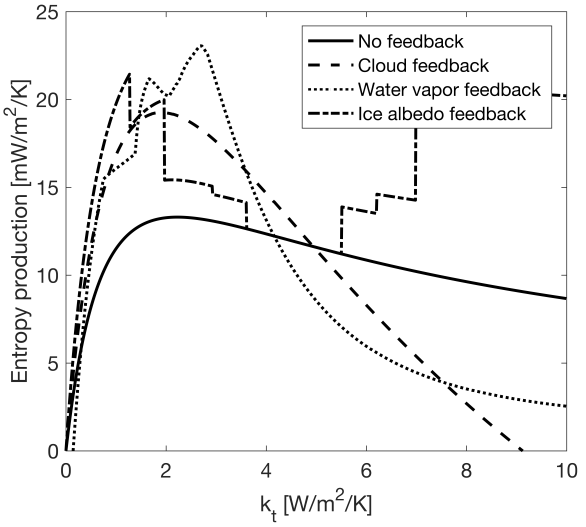

Figure 11: Entropy production as function of our heat transport constant (k_t) for a model setups which considers either no feedback or each feedback mechanism separately.

7.2 Enhancement of entropy production

Entropy production according to Paltridge's method consists of a strong interdependence between positive entropy production in the temperature/polar area, and negative entropy production in the equatorial area. The feedback mechanisms in general result in a lower entropy production in the polar/temperature region, while enhancing entropy production in the equatorial region. As can be seen from Figure 10, the effect the feedback mechanisms have on entropy production manifest themselves particularly in the equatorial regions, resulting in an overall positive effect of the feedback mechanisms on entropy production as seen in Figure 10.

As can be seen in Figure 10, the zonal values of entropy production are quite large compared to the total entropy production. This implies that slight changes in the behavior of the model can result in large differences in the total entropy production. It also shows the sensitivity of the zonal behavior of entropy production within the model, it is critical to determine in which zones certain repercussions, in this case the feedback mechanisms, have the largest impacts. The use of different reference values or parameterization methods could result in quite different results compared to the current model setup. Inclusion of feedback mechanisms in the current model setup result in an enhancement as well as a reduction of entropy production in the model. Because the enhancement of entropy production in the equatorial region is more apparent than the reduction in entropy production in the polar/temperate region, inclusion of feedback mechanisms results in an overall enhancement of the total entropy production. We do have to mention, that the location of increase in entropy production differs for the other two methods. There, the increase is mainly, if at all, present in the temperate zone, while for Paltridge's

method it is in the equatorial zone. We have not yet further explored the main explanations for these differences in behavior of the system for the other two methods.

8 Snowball Earth experiment

Some models indicate that the Earth in the past was once fully covered in ice due to the fact that the solar constant was approximately 25% lower than it is currently (Newman and Rood, 1977). The MEPP has previously been applied to this *"faint young sun paradox"* by constraining the heat flux (Gerard et al., 1990). Results indicated that in order for the model to comply to the MEPP, the heat flux decreases when the solar constant decreases, resulting in warmer tropics and therefore delaying the onset of a full glaciated Earth. Here we have also conducted an experiment in which we constrained the heat transport constant by use of each of the three methods of entropy production separately as well as without constraining the heat transport constant by the MEPP, i.e. using a fixed heat transport constant. When we performed the experiment by use of a fixed heat transport, it showed that with a model setup solely including the ice albedo feedback, a reduction in solar constant of 25.6% was needed in order to create a snowball Earth. In the model setup in which all feedback mechanisms were considered jointly, a reduction in solar constant of just 22.6% resulted in a snowball Earth. This result can be explained by the fact that the water vapor feedback is a positive feedback, which is stronger in our model than the other added negative cloud feedback as aforementioned in subsection 4.2. Therefore, the decrease in temperature due to the lower solar constant is enhanced by the lower water vapor content of the atmosphere. Given that the solar luminosity has increased by roughly 25 % from the initial formation of the Earth up to the present-day (Newman and Rood, 1977), this result indicates the Earth could have seen a full glaciation in its past.

Our results of the experiment in which the heat transport constant was constrained by the MEPP are presented in Figure 12. The first striking result we see is that, based on Paltridge's method, the system does not reach a maximum in entropy production but instead results in a continuous increase of entropy production when the solar constant is decreased. This results is in contrast with Gerard et al. (1990), who successfully applied Paltridge's method to perform the same tests. Gerard did use the model from Paltridge (1975, 1978), which when constrained by the MEPP according to Paltridge's method is able to accurately reproduce the current climate. Our model's optimal simulation of the current climate on the other hand, as previously demonstrated, does not resemble a state of maximum entropy production. while we have already previously demonstrated our model an optimal simulation of temperature does not resemble the MEP state. The other two used methods did behave as was expected, i.e. do show a decrease in k_t and thus the heat flux with as the solar constant decreases.

It is hypothesized that in order to avoid the Earth to become fully covered in ice, a reduced efficiency in heat transport is critical (Gerard et al., 1990). The reduced heat transport enables the preservation of more heat in the tropics, resulting in temperatures in the tropics high enough to keep the Earth from a full glaciation. Figure 12 shows an overall decrease in the heat transport constant when decreasing the solar constant for the methods Lorenz P and B. However, for a decrease in solar constant of roughly 20%, entropy production becomes highly negative for both methods (not visible in the figure). A possible explanation here could be the temperature deviations in our base model at the two poles, as seen in Figure 2. A more detailed analysis of our results showed that these deviations became more extreme with the decreasing solar constant. A further cause of the negative values in entropy production is our method to calculate the meridional heat flux. It became apparent that while decreasing the solar constant in our model, the heat flux often took unrealistic values when constrained by the MEPP. To calculate entropy production according to the methods Lorenz P and B, the heat flux is a critical component, as shown in Equation (15). Thus although the methods of Lorenz P and B do show behavior that would be expected, they show physically impossible behavior when the solar constant is decreased to a certain small value, because the heat transport becomes zero. These model results are thus unsuitable to assess for which solar constant the model would result in a full ice coverage.

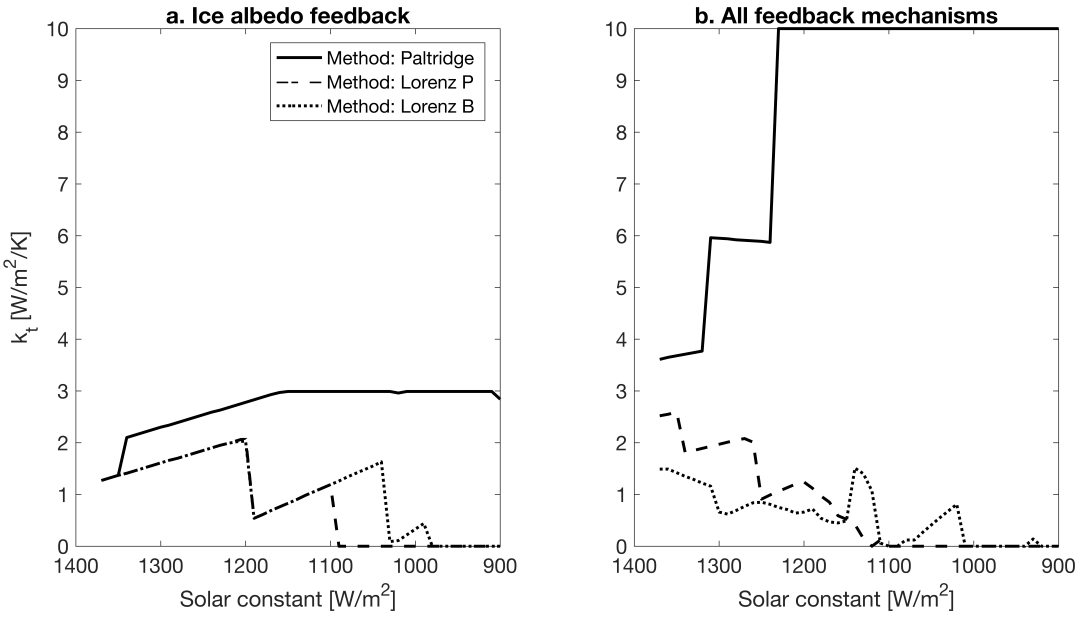

Figure 12: Snowball Earth experiment results. The value of the heat transport constant k_t constrained by the MEPP is plotted for solar constant values ranging from 1370 - 900 W/m^2. Plot a shows the results for the model setup in which only the ice albedo feedback was considered and plot b the results for the model setup in which all feedback mechanisms were considered jointly.

Consequently, we have concluded that we were unable to successfully apply the MEPP in order to explore the faint young sun paradox in our model. An important reason for this could be the fact that we were unable to accurately reproduce the current climate when our model was constrained by the MEPP. A more detailed study could perhaps shed more light on this, particularly a study focused on the method of Paltridge within a Budyko energy balance model. As previously mentioned, local maxima could potentially form an critical feature of the MEPP. Although Paltridge's method was unable to maximize entropy production without a runaway effect, it did show local maxima for values of k_t that are more in line with expectations. As we previously mentioned, the MEPP can possibly better be seen as a direction in which a system evolves. In future studies on exploring the faint young sun paradox by use of MEPP, it can perhaps be of interest to use the evolution of the sun as a way to explore the increase of entropy production over time. Within this study, one can investigate whether entropy production in the Earth's history has evolved from local maxima towards higher local maxima and perhaps currently the highest maximum in entropy production.

9 Conclusion

This paper provides an analysis of how inclusion of feedback mechanisms within an simple equilibrium 18-box energy balance model based on Budyko (1969) affects entropy production due to meridional heat transport. Budyko's model originally already included the ice albedo feedback mechanisms, and is here extended by implementation of both the cloud and water vapor feedback. For the calculation of entropy production, the methods proposed by Paltridge (1975, 1978) and Lorenz et al. (2001) were used and compared to each other, with the main focus being the method by Paltridge. Furthermore have we applied the MEPP to explore whether the Earth was once fully glaciated within its early days. A short evaluation of model simulations showed that our model is able to capture the most salient features of the Earth's climate system when not constrained by the MEPP (see Figure 2.

With the exception of the model setup including all feedback mechanisms and entropy production calculated by use of Paltridge's method, our model was unable to reproduce the current climate when the meridional heat flux was constrained by the MEPP (see . This could partly be due to the model setup. A comparison of our model setup with that from Paltridge for example indicated that certain processes within our model (e.g. the heat flux) are possibly overspecified. Another factor that could play a role is seasonality, e.g. consideration of a seasonal cycle in radiation. Another study has constrained two models by the MEPP and found that in order for both models to accurately simulate the current climate inclusion of seasonality was essential Wyant et al. (1988). A short rework of these proposed effects of including seasonality on the application of the MEPP, is here presented by use of a simple two-box energy balance model. The results from this small experiment showed that including seasonality has an influence on the entropy production within the system and result in an, although small, enhancement of the model's ability to reproduce the current climate. Due to the fact that only a two-box model is used within this study, inclusion of seasonality could have larger repercussions in more complex models.

Although documented more often Noda and Tokioka (1983); Shimokawa and Ozawa (2002); Martyushev and Seleznev (2006); Jupp and Cox (2010); Herbert et al. (2011), the existence of multiple maxima in entropy production is, at least to our knowledge, still not an integral part of the MEPP. Results of this study also indicates the existence of multiple maxima in entropy production within system Earth. The ice albedo feedback mechanism showed here to be imperative for multiple maxima to occur. However, the cloud and water vapor feedback mechanisms were needed in order for the model to result in positive peak values of entropy production. Due to the importance of the ice albedo feedback mechanism for the entropy production to result in the sudden peaks seen within Figure 7, we have implemented a second parameterization of this feedback. This second parameterization showed that as the behavior of the ice albedo feedback becomes less abrupt, entropy production within the model also exhibited a more gradual behavior as function of the heat transport constant k_t (see Figure 8).

A last observed feature of the entropy production within our model is the enhancement of maxima in entropy production when the feedback mechanisms are included within the model runs either individually or all jointly (see Figure 10). Analysis of the behavior of entropy production on a zonal scale showed that the feedback mechanisms cause the entropy production to become less negative within the equatorial region, and therefor result in a higher global maxima in entropy production. Although entropy production according to the second law of thermodynamics can never become negative, negative entropy producion here is a trade-off of the method used and can because of this only be successfully applied when summed globally.

It is suggested that the Earth possibly has once been fully covered in ice in its past due to the solar constant being approximately 25% lower than it is currently Newman and Rood (1977). Here we have investigated when our model, when constrained by the MEPP and when not constrained, would result in a global ice coverage when the solar constant is slowly reduced. Results of the unconstrained model showed a global ice coverage when the solar constant was reduced by 22.6% when all feedback mechanisms were included, indicating that the Earth could have seen a full glaciation in its past. However, when only the ice albedo feedback mechanism was included a solar constant reduction of 25.6% was needed. Our experiment with the model constrained by the MEPP resulted in physically unrealistic values for the heat transport and are therefore untrustworthy.

Our model is able to reproduce the most salient features of Earth's climate when unconstrained. However, when constrained by the MEPP, the model showed to be unable to accurately reproduce the current climate. As has also been previously reported by other studies, but not yet an integral part of the MEPP, entropy production within the model resulted in the occurrence of multiple maxima in entropy production, with the ice albedo feedback mechanism being essential. Besides resulting in multiple maxima, consideration of the feedback mechanisms within the model resulted in an increased maximum in entropy production compared to model runs in which no feedback mechanisms were considered. A short review of literature on

the MEPP combined with the results of our study indicates the notion that the MEPP possibly represents the direction rather than the present day state of the system or perhaps presents the possible steady-state solutions of a system.

References

Budyko, M. I. (1969). The effect of solar radiation variations on the climate of the earth. *Tellus*, 21(5):611–619.

Carissimo, B. and Oort, A. (1985). Estimating the meridional energy transports in the atmosphere and oceans. *J. Phys. Oceanogr*, 15:82–91.

Cess, R. D. (1976). Climate change: An appraisal of atmospheric feedback mechanisms employing zonal climatology. *Journal of the Atmospheric Sciences*, 33(10):1831–1843.

Cess, R. D., Potter, G., Blanchet, J., Boer, G., Del Genio, A., Deque, M., Dymnikov, V., Galin, V., Gates, W., Ghan, S., et al. (1990). Intercomparison and interpretation of climate feedback processes in 19 atmospheric general circulation models. *Journal of Geophysical Research: Atmospheres*, 95(D10):16601–16615.

Chỳlek, P. and Coakley Jr, J. (1975). Analytical analysis of a budyko-type climate model. *Journal of the Atmospheric Sciences*, 32(4):675–679.

Dewar, R. (2003). Information theory explanation of the fluctuation theorem, maximum entropy production and self-organized criticality in non-equilibrium stationary states. *Journal of Physics A: Mathematical and General*, 36(3):631.

Dewar, R. C. (2005). Maximum entropy production and the fluctuation theorem. *Journal of Physics A: Mathematical and General*, 38(21):L371.

Dyke, J. G. (2008). Entropy production in an energy balance daisyworld model.

Gerard, J.-C., Delcourt, D., and Francois, L. M. (1990). The maximum entropy production principle in climate models: application to the faint young sun paradox. *Quarterly Journal of the Royal Meteorological Society*, 116(495):1123–1132.

Golitsyn, G. and Mokhov, I. (1978). Stability and extremal properties of climate models. *Academy of Sciences, USSR, Izvestiya, Atmospheric and Oceanic Physics*, 14:271–277.

Goody, R. (2007). Maximum entropy production in climate theory. *Journal of the atmospheric sciences*, 64(7):2735–2739.

Grassl, H. (1981). The climate at maximum entropy production by meridional atmospheric and oceanic heat fluxes. *Quarterly Journal of the Royal Meteorological Society*, 107(451):153–166.

Hall, A. and Manabe, S. (1999). The role of water vapor feedback in unperturbed climate variability and global warming. *Journal of climate*, 12(8):2327–2346.

Hartmann, D., Klein Tank, A., Rusticucci, M., Alexander, L., Brönnimann, S., Charabi, Y., Dentener, F., Dlugokencky, E., Easterling, D., Kaplan, A., Soden, B., Thorne, P., Wild, M., and Zhai, P. (2013). *Observations: Atmosphere and Surface*, book section 2, page 159–254. Cambridge University Press, Cambridge, United Kingdom and New York, NY, USA.

Haurwitz, B. and James, M. (1944). Austin, climatology. *McGraw-Hill, New York*, 191(4):I4.

Hazeleger, W., Wang, X., Severijns, C., Ştefănescu, S., Bintanja, R., Sterl, A., Wyser, K., Semmler, T., Yang, S., Van den Hurk, B., et al. (2012). Ec-earth v2. 2: description and validation of a new seamless earth system prediction model. *Climate Dynamics*, 39(11):2611–2629.

Held, I. M. and Soden, B. J. (2000). Water vapor feedback and global warming 1. *Annual review of energy and the environment*, 25(1):441–475.

Herbert, C., Paillard, D., and Dubrulle, B. (2011). Entropy production and multiple equilibria: the case of the ice-albedo feedback. *arXiv preprint arXiv:1103.0722*.

Jupp, T. E. and Cox, P. M. (2010). Mep and planetary climates: insights from a two-box climate model containing atmospheric dynamics. *Philosophical*

Transactions of the Royal Society of London B: Biological Sciences, 365(1545):1355–1365.

Kiehl, J. T. and Trenberth, K. E. (1997). Earth's annual global mean energy budget. *Bulletin of the American Meteorological Society*, 78(2):197–208.

Kleidon, A. (2004). Beyond gaia: thermodynamics of life and earth system functioning. *Climatic Change*, 66(3):271–319.

Kleidon, A. (2009). Nonequilibrium thermodynamics and maximum entropy production in the earth system. *Naturwissenschaften*, 96(6):1–25.

Kleidon, A. (2010). A basic introduction to the thermodynamics of the earth system far from equilibrium and maximum entropy production. *Philosophical Transactions of the Royal Society of London B: Biological Sciences*, 365(1545):1303–1315.

Kleidon, A. (2012). How does the earth system generate and maintain thermodynamic disequilibrium and what does it imply for the future of the planet? *Phil. Trans. R. Soc. A*, 370(1962):1012–1040.

Kleidon, A., Fraedrich, K., Kunz, T., and Lunkeit, F. (2003). The atmospheric circulation and states of maximum entropy production. *Geophysical research letters*, 30(23).

Kleidon, A., Malhi, Y., and Cox, P. M. (2010). Maximum entropy production in environmental and ecological systems. *Philosophical Transactions of the Royal Society of London B: Biological Sciences*, 365(1545):1297–1302.

Lagarias, J. C., Reeds, J. A., Wright, M. H., and Wright, P. E. (1998). Convergence properties of the nelder–mead simplex method in low dimensions. *SIAM Journal on optimization*, 9(1):112–147.

Lian, M. and Cess, R. (1977). Energy balance climate models: A reappraisal of ice-albedo feedback. *Journal of the Atmospheric Sciences*, 34(7):1058–1062.

Lorenz, R. D. (2002). Planets, life and the production of entropy. *International Journal of Astrobiology*, 1(01):3–13.

Lorenz, R. D. (2010). The two-box model of climate: limitations and applications to planetary habitability and maximum entropy production studies. *Philosophical Transactions of the Royal Society of London B: Biological Sciences*, 365(1545):1349–1354.

Lorenz, R. D., Lunine, J. I., Withers, P. G., and McKay, C. P. (2001). Titan, mars and earth: Entropy production by latitudinal heat transport. *Geophysical Research Letters*, 28(3):415–418.

Lovelock, J. E. (1965). A physical basis for life detection experiments. *Nature*, 207(997):568–570.

Lovelock, J. E. and Kaplan, I. (1975). Thermodynamics and the recognition of alien biospheres [and discussion]. *Proceedings of the Royal Society of London B: Biological Sciences*, 189(1095):167–181.

Martyushev, L. and Seleznev, V. (2006). Maximum entropy production principle in physics, chemistry and biology. *Physics reports*, 426(1):1–45.

Meysman, F. J. and Bruers, S. (2010). Ecosystem functioning and maximum entropy production: a quantitative test of hypotheses. *Philosophical Transactions of the Royal Society of London B: Biological Sciences*, 365(1545):1405–1416.

Myhre, G., Shindell, D., Bréon, F.-M., Collins, W., Fuglestvedt, J., Huang, J., Koch, D., Lamarque, J.-F., Lee, D., Mendoza, B., Nakajima, T., Robock, A., Stephens, G., Takemura, T., and Zhang, H. (2013). *Anthropogenic and Natural Radiative Forcing*, book section 8, page 659–740. Cambridge University Press, Cambridge, United Kingdom and New York, NY, USA.

Nelder, J. A. and Mead, R. (1965). A simplex method for function minimization. *The computer journal*, 7(4):308–313.

Newman, M. J. and Rood, R. T. (1977). Implications of solar evolution for the earth's early atmosphere. *Science*, 198(4321):1035–1037.

Nicolis, B. G. and Nicolis, C. (1980). On the entropy balance of the earth-atmosphere system. *Quarterly Journal of the Royal Meteorological Society*, 106(450):691–706.

Noda, A. and Tokioka, T. (1983). Climates at minima of the entropy exchange rate. *Journal of the Meteorological Society of Japan. Ser. II*, 61(6):894–908.

North, G., Short, D., and Mengel, J. (1983). Simple energy balance model resolving the seasons and the continents- application to the astronomical theory of the ice ages. *Journal of Geophysical Research*, 88(C11):6576–6586.

North, G. R., Cahalan, R. F., and Coakley, J. A. (1981). Energy balance climate models. *Reviews of Geophysics*, 19(1):91–121.

North, G. R. and Coakley Jr, J. A. (1979). Differences between seasonal and mean annual energy balance model calculations of climate and climate sensitivity. *Journal of the Atmospheric Sciences*, 36(7):1189–1204.

O'brien, D. and Stephens, G. (1995). Entropy and climate. ii: Simple models. *Quarterly Journal of the Royal Meteorological Society*, 121(527):1773–1796.

Ozawa, H., Ohmura, A., Lorenz, R. D., and Pujol, T. (2003). The second law of thermodynamics and the global climate system: a review of the maximum entropy production principle. *Reviews of Geophysics*, 41(4).

Paltridge, G. (1978). The steady-state format of global climate. *Quarterly Journal of the Royal Meteorological Society*, 104(442):927–945.

Paltridge, G. W. (1975). Global dynamics and climate-a system of minimum entropy exchange. *Quarterly Journal of the Royal Meteorological Society*, 101(429):475–484.

Paltridge, G. W., Farquhar, G. D., and Cuntz, M. (2007). Maximum entropy production, cloud feedback, and climate change. *Geophysical Research Letters*, 34(14).

Pascale, S., Gregory, J., Ambaum, M. H., Tailleux, R., and Lucarini, V. (2012). Vertical and horizontal processes in the global atmosphere and the maximum entropy production conjecture. *Earth System Dynamics*, 3(1):19–32.

Peixoto, J. P., Oort, A. H., De Almeida, M., and Tomé, A. (1991). Entropy budget of the atmosphere. *Journal of Geophysical Research: Atmospheres*, 96(D6):10981–10988.

Porada, P., Kleidon, A., and Schymanski, S. (2011). Entropy production of soil hydrological processes and its maximisation. *Earth System Dynamics*, 2(2):179–190.

Pujol, T. (2002). The consequence of maximum thermodynamic efficiency in daisyworld. *Journal of theoretical biology*, 217(1):53–60.

Sellers, W. D. (1965). Physical climatology. Technical report, University of Chicago Press.

Shimokawa, S. and Ozawa, H. (2002). On the thermodynamics of the oceanic general circulation: Irreversible transition to a state with higher rate of entropy production. *Quarterly Journal of the Royal Meteorological Society*, 128(584):2115–2128.

Su, C. and Hsieh, D. (1976). Stability of the budyko climate model. *Journal of the Atmospheric Sciences*, 33(12):2273–2275.

Trenberth, K. E., Fasullo, J. T., and Kiehl, J. (2009). Earth's global energy budget. *Bulletin of the American Meteorological Society*, 90(3):311.

Walsh, J. and Rackauckas, C. (2015). On the budyko–sellers energy balance climate model with ice line coupling. *Disc. Cont. Dyn. Syst.*, 20.

Wyant, P., Mongroo, A., and Hameed, S. (1988). Determination of the heat-transport coefficient in energy-balance climate models by extremization of entropy production. *Journal of the atmospheric sciences*, 45(2):189–193.

Appendices

A Table: variables of the model

Table 6: Parameters with their corresponding values and units used in the model.

Symbol	Value/unit	Variable
Q	1370 [W/m^2]	Solar constant
Q_i	[W/m^2]	Zonal incoming radiation
$F_{in,i}$	[W/m^2]	Zonal net incoming shortwave radiation at TOA
$F_{in,wv,i}$	[W/m^2]	Zonal incoming radiation from both the sun and water vapor feedback
$F_{out,i}$	[W/m^2]	Zonal outgoing longwave radiation at TOA
Wv	0.8409* [W/m^2]	Average zonal LW radiation absorption constant of the atmosphere
$T_{s,i}$	[K]	Average zonal surface temperature
T_s0	[K]	Average zonal reference temperature
T_p	[K]	Average planetary surface temperature
T_h	[K]	Calculated reference temperature with respect to one of the feedback mechanisms
$T_{a,i}$	[K]	Average zonal temperature at TOA
α_p		Average global albedo
α_z		Average zonal albedo
$\alpha_{c,i}$		Average atmospheric zonal albedo
$\alpha_{s,i}$		Average zonal surface albedo
αice	0.61	Albedo of ice
$\alpha 0, i$		Reference zonal surface albedo
C_c	[%]	Average zonal cloud cover
A_n	204 [W/m^2]	Temperature tuning parameter for the northern hemisphere
B_n	2.10 [W/m^2/K]	Temperature tuning parameter for the northern hemisphere
A_s	206 [W/m^2]	Temperature tuning parameter for the southern hemisphere
B_s	2.2 [W/m^2/K]	Temperature tuning parameter for the southern hemisphere
k_t	3.81[W/m^2/K]	Heat transport constant
k_s	0.14	Tuning parameter determining the slope at which albedo increases
a_{Cc}	0.061	Tuning parameter for the cloud feedback
a_{wv}	0.061	Tuning parameter for the water vapor feedback
$Cc_{0,i}$	[%]	Reference cloud cover for each zone
$Wv_{0,i}$	[W/m^2]	Average zonal reference LW radiation absorption constant of the atmosphere
G	0.4 [%]	Fraction of longwave radiation loss to space by a cloud-free atmosphere
ϵ'	0.75	Constant of the atmospheric window to IR
f	0.8 [%]	Fraction reduced black-body radiation from clouds
F_{hf}	[W/m^2]	Zonal difference in heat due to meridional heat transport
S_{hf}	[W/m^2/K]	Entropy production due to meridional heat transport
σ	5.67^{-8} [W/m^2/K]	The Stefan–Boltzmann constant

B Two-box model: inclusion of time dependence

Wyant et al. (1988) studied the application of MEPP in simple energy balance climate models from a different angle. They chose to look at models including seasonality instead of average equilibrium models used for example in the studies by Paltridge (1975, 1978); Nicolis and Nicolis (1980); Grassl (1981); Gerard et al. (1990); Lorenz et al. (2001) and in this study. They concluded time dependence, e.g. consideration of the seasonal cycle in radiation, to be essential for successful application of MEPP in simple energy balance models.

Our equilibrium model showed to be unsuccessful in the application of MEPP, in particular when the model did not include all feedback mechanisms simultaneously. The same conclusion was reached previously by Golitsyn and Mokhov (1978) (as cited in Wyant et al., 1988) who used a similar Budyko-Sellers type energy balance model. The results of Wyant et al. (1988) propose a potential incentive as to why. Their study concluded that inclusion of time dependence was essential in the models they used in order to reproduce the current climate when the model was constrained by the MEPP. Further exploration of this idea could be of interest in explaining the results found here and previously by Golitsyn and Mokhov (1978) (as cited in Wyant et al., 1988).

We would like to test the validity and extend of this idea here. For simplicity we have chosen, instead of applying seasonality to our previously described Budyko-type model (by use of the study by North and Coakley Jr (1979) for example), to apply it to a comparable two-box energy balance model depicted in Figure 13. The model, similar as the modeling approach according to Lorenz et al. (2001), distinguishes two boxes of equal surface area covering together the whole northern hemisphere. One box represents the equatorial region and the other the temperate/polar region. Each box was subsequently divided into two layers, a surface and an atmospheric layer.

For both layers in each box, differential equations are used to calculate the change in temperatures compared to the previous time step and is subsequently added each iteration to the previous temperature to calculate the new temperature. The model used time steps

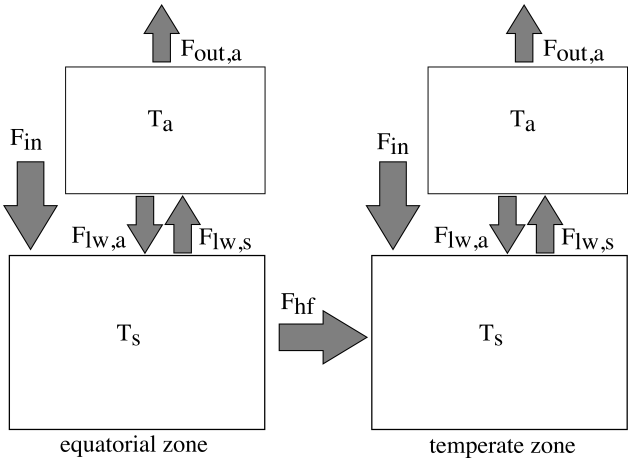

Figure 13: Overview of the model setup used to test the effects of including seasonality, e.g. a seasonal cycle in radiation, on the MEPP.

of days, and ran for a period of 10 years. The change in temperature is calculated by dividing the change in heat by the heat capacity of either the surface or the atmosphere. The heat capacity of the surface takes into account differing heat capacities of the ocean, bare surface, and when covered by ice or snow. The basic equation to determine the change in temperature is:

$$\frac{dT}{dt} = (R_{net} + -F_{hf})/C, \tag{18}$$

in which F_{hf} represents the added heat due to the heat transport between the boxes, which is for the equatorial boxes negative and for the polar box positive. The heat transport is defined as $F = k_t \Delta T_s$ within the model. R_{net} represents the net radiation of the box, which is calculated for the surface through:

$$R_{net,s} = F_{in} + F_{lw,a} - F_{lw,s}, \tag{19}$$

where F_{in} represents the net incoming shortwave radiation, $F_{lw,a}$ the incoming longwave radiation from the atmosphere (i.e. greenhouse effect), and $F_{lw,s}$ the outgoing longwave radiation from the surface. For the atmosphere $R_{net,a}$ is calculated through:

$$R_{net,a} = F_{lw,s} - F_{lw,a} - F_{out,a} \tag{20}$$

where $F_{out,a}$ denotes the outgoing longwave radiation from the atmosphere to space. Customarily, one would add the heat due to the heat flux between both boxes

to the atmospheric layer, however here it is chosen to add it to the heat balance of the surface layer to enable comparison of the methodology and results with that from Lorenz et al. (2001) for model validation purposes (e.g. comparison of values for the heat transport constant). Seasonality is created within the model by applying a sine function to the incoming shortwave radiation at the top of the atmosphere, F_{in}.

Apart from the heat transport, all variables and constants in the model are fixed, the model does not contain any feedback mechanisms. The heat transport within the model was constrained by the MEPP, with entropy production of the model being calculated according to Lorenz et al. (2001):

$$S = F_{hf}(\frac{1}{Ts, cold} - \frac{1}{Ts, hot}). \qquad (21)$$

Two runs were conducted with the model, the only difference being the activation of seasonality.